LITHOS 428–429 (2022) 106808

Contents lists available at ScienceDirect

LITHOS

journal homepage: www.elsevier.com/locate/lithos

# Petrogenesis of low-pressure intra-oceanic arc granitoids: Insights from the late Neoproterozoic Avalonian–Cadomian orogen, Bohemian Massif

Václav Santolík [a,b,*], Lukáš Ackerman [a], Václav Kachlík [c], Jiří Sláma [a], Noemi Mészárosová [a]

[a] Institute of Geology of the Czech Academy of Sciences, Rozvojová 269, Prague 6 165 00, Czech Republic
[b] Institute of Geochemistry, Mineralogy and Mineral Resources, Faculty of Science, Charles University, Albertov 6, Prague 2 128 43, Czech Republic
[c] Institute of Geology and Paleontology, Faculty of Science, Charles University, Albertov 6, Prague 2 128 43, Czech Republic

ARTICLE INFO

*Keywords:*
Intra-oceanic island arc
Trondhjemite
Juvenile crust
Inverse geochemical modelling
Fractional crystallization
Partial melting

ABSTRACT

The processes leading to the formation of siliceous (intermediate to felsic) magmatic rocks from juvenile sources within intra-oceanic island arcs govern the formation of continental crust and tempos of crustal growth. To unravel the predominant process responsible for the formation of the intermediate to felsic intra-oceanic arc crust, we performed inverse geochemical modelling using major elements and fluid-immobile trace elements. Subvolcanic trondhjemite from a volcanic arc – Davle volcanic complex (DVC) situated in the Teplá–Barrandian unit, Bohemian Massif – that formed during the Neoproterozoic Avalonian–Cadomian orogeny was used as a proxy for the most felsic endmember of the tonalite–trondhjemite suite. The DVC trondhjemite that follows the calc-alkaline trend is enriched in several fluid-mobile elements such as Cs, Ba and U, but depleted in high field strength elements (Nb, Ti) and lithophile elements (e.g., K, Rb, Sr and Th), and exhibits flat rare earth element (REE) primitive mantle-normalized distributions with slightly negative Eu anomalies. Together with the largely radiogenic Hf-Nd isotopic signatures ($\varepsilon_{Nd}$ +6.0 to +8.7 and $\varepsilon_{Hf}$ +10.2 to +11.7), these data indicate formation in an intra-oceanic arc setting with no significant assimilation of older crustal material. In general, the composition of the studied trondhjemite markedly resembles that of other intra-oceanic arc-derived tonalites and trondhjemites worldwide, formed at low pressures below the garnet stability field. These are herein referred to as "low-pressure intra-oceanic arc granitoids" or "LP IOAG". The performed inverse geochemical modelling revealed that dehydration partial melting or fractional crystallization of a mafic source can produce a primitive tonalitic melt. Consequently, fractional crystallization of that melt accounts for the compositional heterogeneity observed within the tonalite–trondhjemite suite. We conclude that LP IOAG, commonly forming large portions of intra-oceanic arc middle crust, can form in a nearly closed system with a negligible contribution of subduction-related melts or assimilation of older siliceous crust. Therefore, our findings suggest that the formation of LP IOAG within oceanic crust may represent the predominant process of post-Archean crustal growth.

## 1. Introduction

The principles of crustal growth are a hot topic within the modern geological community (Marien et al., 2022; Moyen et al., 2021; Moyen and Martin, 2012; Stern and Scholl, 2010). While high-pressure melting of basaltic crust was likely the major process of continental crust growth during the Archean (Castillo, 2012; Martin et al., 2005; Moyen and Martin, 2012; Stern and Scholl, 2010), the processes of post-Archean crustal growth involve a significant proportion of crustal recycling (Jagoutz, 2010; Moyen et al., 2021). However, seismic velocity profiles of intra-oceanic island-arc crust revealed low-velocity middle crust supposedly composed of intermediate to felsic igneous rocks (Calvert, 2011). Combined with evidence from exposed ancient island arcs, it is assumed that large portions of siliceous crust can be formed within intra-oceanic arcs, where no continental crust is available to be recycled (DeBari and Greene, 2011; Greene et al., 2006; Kawate and Arima, 1998). These juvenile igneous intermediate to felsic rocks (tonalite, trondhjemite and equivalent volcanic products) can provide unique insights into the processes governing the post-Archean formation of siliceous continental crust (Beard, 1995; DeBari and Greene, 2011; Frost et al., 2016; Greene et al., 2006; Jagoutz, 2010; Kelemen et al., 2003; Moyen et al., 2021; Stern and Scholl, 2010).

* Corresponding author at: Institute of Geology of the Czech Academy of Sciences, Rozvojová 269, Prague 6 165 00, Czech Republic.
*E-mail address:* vsantolik@gmail.com (V. Santolík).

https://doi.org/10.1016/j.lithos.2022.106808
Received 5 March 2022; Received in revised form 30 June 2022; Accepted 16 July 2022
Available online 23 July 2022
0024-4937/© 2022 Elsevier B.V. All rights reserved.

Rare earth element (REE) and high field strength element (HFSE) geochemical modelling represents a powerful tool to understand the nature and succession of petrogenetic processes related to the formation of intra-oceanic arc crust (Greene et al., 2006; Kawate and Arima, 1998; Rollinson, 1993, 2009). For example, steep REE patterns (high $La_N/Yb_N$) typical of Archean tonalite–trondhjemite–granodiorite (TTG) suites and post-Archean adakites argue for partial melting at high pressures (>1 GPa) in the presence of garnet in the residue (Castillo, 2012; Martin et al., 2005; Moyen, 2009; Moyen and Martin, 2012). Nevertheless, most of the voluminous low-K intermediate/felsic plutons of middle crust of intra-oceanic arcs as well as the associated andesites, dacites and rhyolites show rather flat REE patterns (Gill, 1981; Greene et al., 2006; Kawate and Arima, 1998; Kelemen et al., 2003; Leat et al., 2007) suggesting a limited role of garnet and hence lower pressures (<1 GPa). Additionally, other studies highlighted the importance of amphibole fractionation that can equally derive high $La_N/Yb_N$ ratios but produces low (≤1) $Dy_N/Yb_N$ ratios with typical convex REE patterns, as documented by Dy/Dy* < 1 in the fractionated melt (e.g., Bédard, 2006; Davidson et al., 2013).

Some REEs and HFSEs show anomalous concentrations relative to neighbouring elements with similar compatibilities, indicating fractionation of a certain mineral. For instance, europium, as the only REE with valence 2+ in addition to 3+, can substitute for $Ca^{2+}$ in plagioclase; therefore, its behaviour indicates plagioclase fractionation/accumulation (e.g., Rollinson, 1993). Titanium, niobium and tantalum show negative anomalies in arc magmas since they are compatible in Fe-Ti oxides which become swiftly saturated in the oxidized environment of subduction zones and therefore fractionate (Chin et al., 2018; Foley et al., 2000). Negative or positive anomalies in the concentration of phosphorus are controlled by the fractionation of apatite.

In this study, we present detailed petrography and bulk rock major/trace element data as well as isotopic (Hf-Nd) geochemical data for several samples of trondhjemite representing a characteristic member of a well-preserved remnant of a Neoproterozoic intra-oceanic island arc (Davle volcanic complex; DVC). It is a part of the Teplá–Barrandian unit of the Bohemian Massif and is related to the Avalonian–Cadomian accretionary orogeny (Ackerman et al., 2019; Drost et al., 2011; Franke, 2006; Hajná et al., 2011; Waldhauserová, 1984; Fig. 1A). Based on the obtained data and inverse geochemical modelling for major elements and fluid-immobile trace elements (REEs, HFSEs and Th), we attempt to unravel the process of DVC trondhjemite petrogenesis, which may be applicable also to similar arc-related rocks in general.

## 2. Geological setting

The Bohemian Massif, formed during the late Paleozoic Variscan orogeny, was amalgamated from several crustal segments including the Teplá–Barrandian unit (Faryad and Kachlík, 2013; Franke, 2006; Hajná et al., 2011; Žák and Sláma, 2018; Žák et al., 2014; Fig. 1B). The Teplá–Barrandian unit (TBU) was in an upper-plate position between the Moldanubian unit to the SE (present-day coordinates) and Saxothuringian unit to the NW (present-day coordinates). It was intruded by the Central Bohemian plutonic complex (CBPC) at the border with the Moldanubian unit during the Variscan orogeny. As a result, the Neoproterozoic and early Paleozoic rocks of the TBU form the roof of the CBPC (Franke, 2006; Žák et al., 2014). Compared to other units, the majority of the TBU was only little affected by Variscan metamorphism due to its upper-plate position, and therefore represents probably the best preserved and best exposed transect of the Neoproterozoic Cadomian active margin that developed north of the Gondwana supercontinent (Ackerman et al., 2019; Drost et al., 2011; Hajná et al., 2011).

The TBU consists of four main parts, from NW to SE: (1) the Mariánské Lázně ophiolite complex comprising amphibolite, metagabbro, eclogite and serpentinized spinel peridotite altogether standing as a remnant of the subducting oceanic plate (Collett et al., 2022), (2) the Blovice accretionary complex composed of greywacke, shale, siltstone and basalt accompanied by minor black shale, carbonate and chert (Ackerman et al., 2019; Hajná et al., 2014), (3) the Davle volcanic complex (DVC) consisting of volcanic/subvolcanic and volcanosedimentary rocks and representing a relic of a volcanic arc (Hajná et al., 2011; Waldhauserová, 1984), and (4) the overlying Štěchovice Group and Svrchnice Formation sedimentary rocks deposited in post-volcanic intra-arc and back-arc sedimentary basins, respectively (Hajná et al., 2011; Sláma et al., 2008).

The DVC is exposed in several anticlinal structures from beneath the Štěchovice Group sedimentary succession (Ackerman et al., 2021; Hajná et al., 2011; Fig. 1C). It is formed by volcanic/volcaniclastic/pyroclastic and subvolcanic/plutonic rocks. Volcanic rocks cover a wide compositional field of rhyolite, dacite, andesite, and rare andesite/basaltic andesite pillow lavas, whereas volcaniclastic and pyroclastic rocks are dominated by rhyolitic and dacitic agglomerates, tuffs and ash flows. Several trondhjemite bodies were emplaced at the base of the volcanic succession as a subvolcanic/plutonic member of the DVC (Fediuk, 2004; Morávek and Röhlich, 1971; Waldhauserová, 1984; Fig. 2A, B). These rocks, targeted in this study, are predominantly exposed in the centre of the largest anticline structure (frequently referred to as the Jílové belt, e.g., Hajná et al., 2011; Waldhauserová, 1984) but also occur in small (<1 km) bodies mapped in the easternmost part of the Blovice accretionary complex (the Pičín belt; Hajná et al., 2011). Trondhjemite was discordantly emplaced to stratigraphically lower members of the DVC basaltic andesite to andesite lavas. These were commonly incorporated into the trondhjemite body in the form of screens up to several metres thick during the Variscan transpressional anastomosing deformation (Fig. 3A).

The onset of volcanic activity in the DVC is a subject to debate since a direct geologic record is missing; however, the termination of volcanic activity at ~580–560 Ma has been well documented by U-Pb zircon dating of the uppermost DVC rhyolite volcaniclastics and the overlying Štěchovice Group and Svrchnice Formation turbidite successions (Ackerman et al., 2021; Dörr et al., 2002; Drost et al., 2011; Hajná et al., 2011; Hajná et al., 2018; Sláma et al., 2008; Waldhauserová, 1984). Zircon U-Pb ages from rhyolite and trondhjemite pebbles from the overlying sedimentary rocks indicate that the DVC was active at least at 610 to ~568 Ma (Dörr et al., 2002; Sláma et al., 2008; Fig. 2B). It is, however, important to note that the DVC trondhjemite has not been successfully dated yet due to the lack of zircons. Nevertheless, the geochemical and modal similarities of the rhyolitic lavas/tuffs with the trondhjemite suggest that these magmatic rocks belong to the final ~580–560 Ma pulse of magmatic activity in the DVC.

## 3. Samples and methods

Altogether seven samples of trondhjemite were collected from outcrops in the northern part of the DVC (Figs. 1C, 2A), and their GPS coordinates are given in Supplementary Table 1. The sampling sites were selected to encompass the several sections of trondhjemite occurrence, hence, to cover the possible textural/chemical heterogeneity. This sample set was supplemented by the collection of spatially associated mafic DVC pillow lavas. Handling and plotting of major/trace element data and isotopic data employed R-based GCDkit software (Janoušek et al., 2006) while REE modelling was performed using a self-made Microsoft Excel™ spreadsheet.

### 3.1. Plagioclase cathodoluminescence imaging

Cathodoluminescence imaging of plagioclase was carried out at the Faculty of Science, Charles University, Prague, using field emission gun electron probe micro-analyser (FEG-EPMA JXA-8530F, JEOL) and a panchromatic cathodoluminescence detector with 15 kV accelerating voltage and 60 nA probe current. Major element composition of plagioclase was obtained using the JEOL 8230 electron microprobe analyser equipped with five WDS detectors and one EDS detector housed

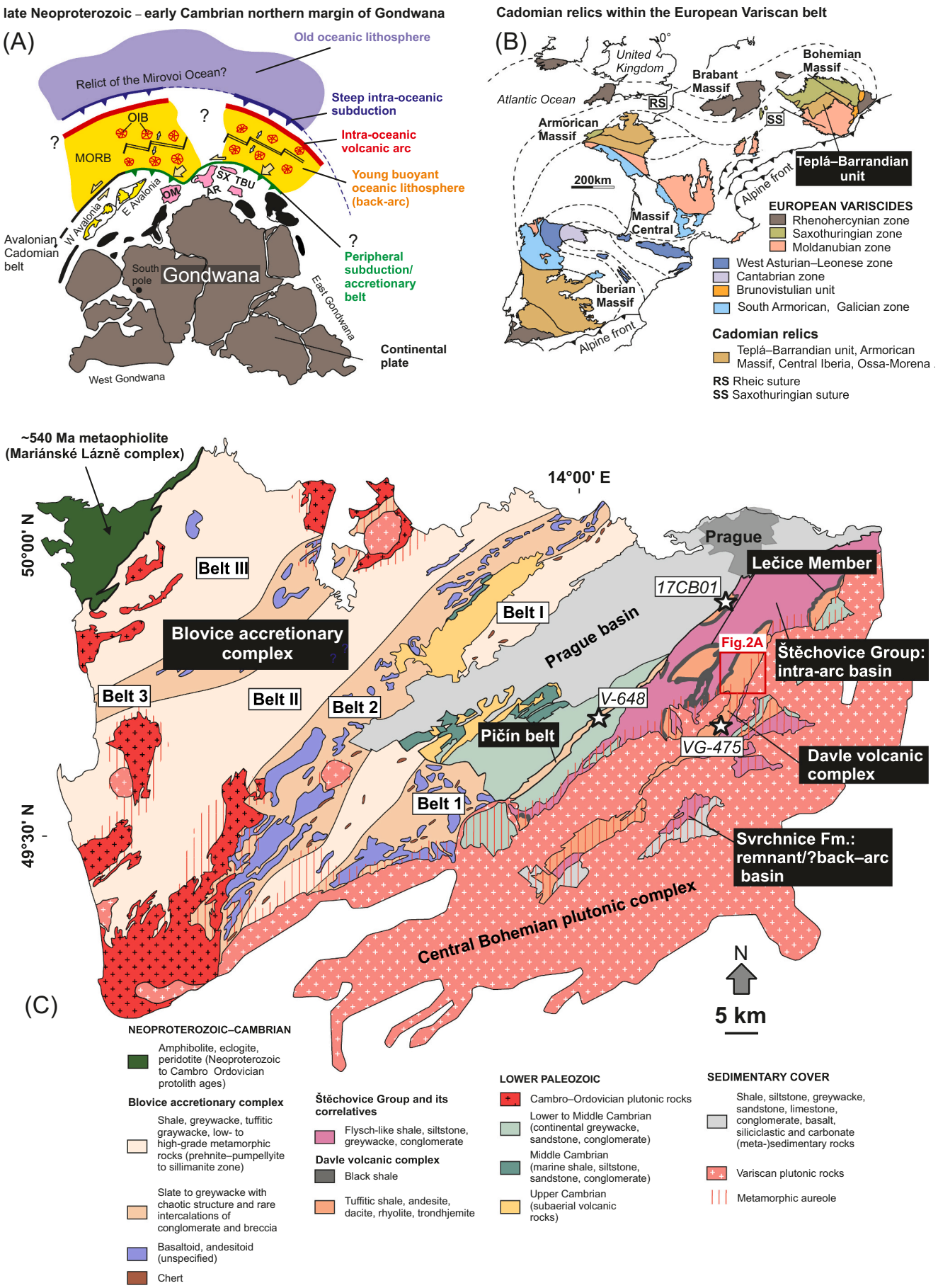


(caption on next page)

**Fig. 1.** (A) Palinspastic reconstruction of the Avalonian–Cadomian orogenic belt on the northern active margin of Gondwana during the late Neoproterozoic; OM – Ossa Morena, AR – Armorican Massif, SX – Saxothuringian unit, TBU – Teplá–Barrandian unit, after Ackerman et al. (2019). (B) An overview of Cadomian terranes incorporated in the European Variscan belt, after Hajná et al. (2014) and references therein. (C) A simplified geological map of the Teplá–Barrandian unit, after Hajná et al. (2014) and references therein, with marked locations of the collected samples.

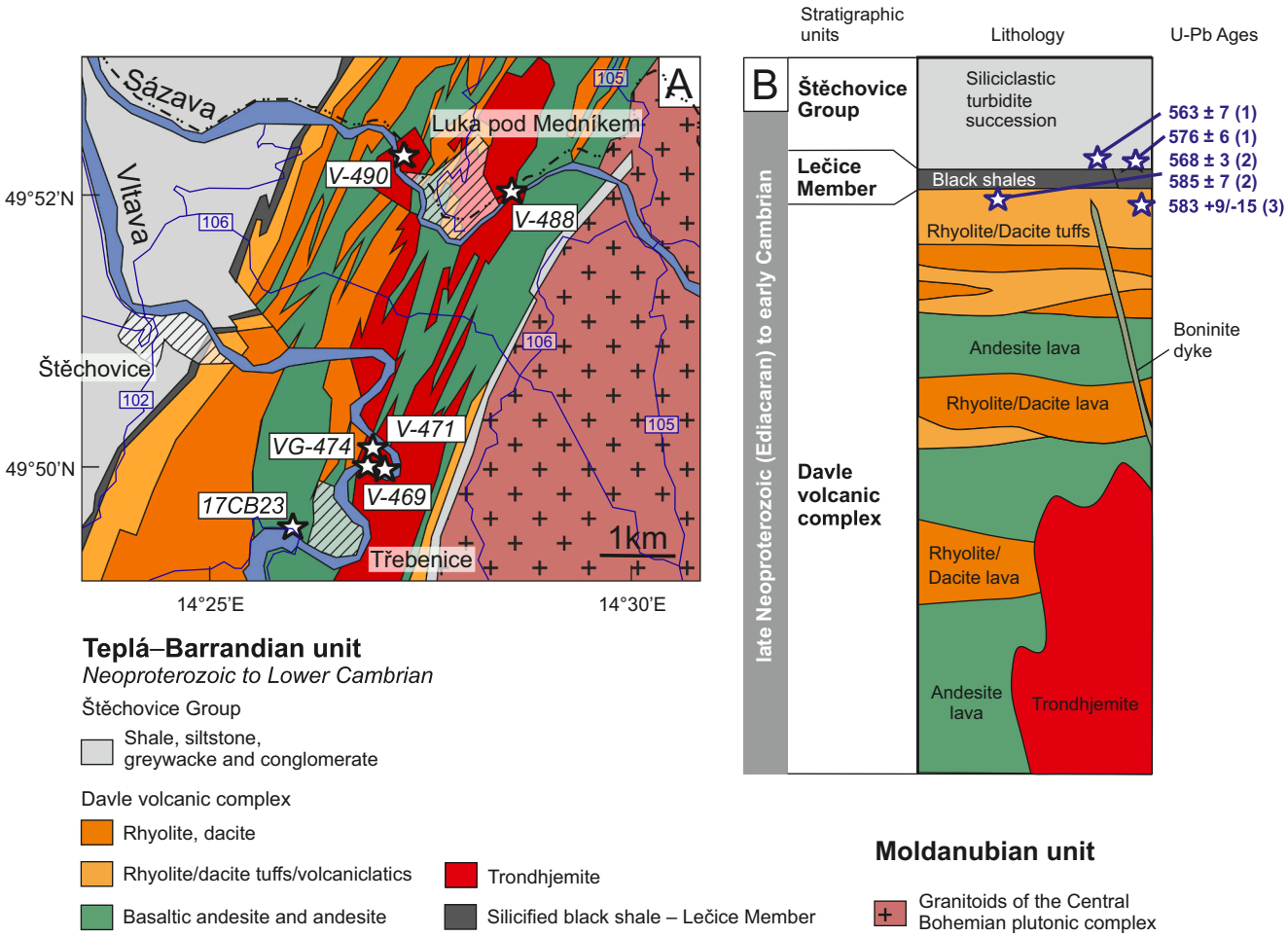


**Fig. 2.** (A) Geological map of the northern part of the Davle volcanic complex (DVC), re-drafted from the geological map of the Czech Republic 1:50,000 published by the Czech Geological Survey, with marked locations of the collected samples. (B) A simplified stratigraphic scheme of the northern part of the DVC, modified after Ackerman et al. (2021). U-Pb ages come from: (1) Hajná et al. (2018), (2) Dörr et al. (2002), (3) Ackerman et al. (2021).

at the Institute of Geology of the Czech Academy of Sciences in Prague (IG CAS). Different natural minerals and synthetic materials were used as standards for the analysis (Supplementary Table 2a). The analytical conditions were as follows: 15 kV accelerating voltage, 10 nA probe current and 2 μm beam diameter. The mineral formulae recalculation was based on 32 O atoms per formula unit. Compositional mapping of Ca, Na and K was performed using the TESCAN VEGA3XMU scanning electron microscope (SEM) housed at the IG CAS.

### 3.2. Bulk rock major and trace elements

Major element concentrations of bulk rock samples were determined at the Faculty of Science, Charles University, and the Czech Geological Survey, Prague. Approximately 0.5 kg of rock was crushed by an iron-jaw crushing machine, quartered and subsequently homogenized in an agate grinder. The analyses followed the wet-chemical procedure described by, e.g., Dempírová et al. (2010). The precision of the analyses was better than ±5%, and the accuracy, monitored by analyses of SY-4 syenite reference material (CANMET), was in good agreement (±8%) with published data (Jochum and Nohl, 2008). Trace element concentrations were determined at the Faculty of Science, Charles University, using the analytical procedure described by Strnad et al. (2005). It involved dry ashing at 700 °C, modified sample digestion in mineral acids (HF–$HClO_4$) and borate fusion ($Na_2CO_3$ + $Na_2B_4O_7$) in Pt crucibles, and subsequent solution ICP-MS analyses (Thermo iCAP-Q). The precision of the analyses for all elements was better than ±5% while the accuracy, monitored by analyses of BCR-2 basalt reference material (USGS), was in excellent agreement (<10%) with published data (Jochum and Nohl, 2008). Only Cs and Ni contents were ~ 20% lower than recommended, while Nb and Hf contents were ~ 20% higher than recommended.

### 3.3. Bulk rock Nd and Hf isotopes

Neodymium isotope compositions were determined at the IG CAS following the method described by Pin et al. (2014). Approximately 150 mg of each sample along with an appropriate amount of $^{150}$Nd-$^{149}$Sm spike were decomposed in a mixture of concentrated HF-$HNO_3$ at 140 °C, dried down, and the residues were re-fluxed several times using concentrated $HNO_3$ and HCl. Subsequently, Nd and Sm were extracted from the solution by ion chromatography using a combination of TRU resin (Triskem France) for bulk REE isolation from the matrix and LN

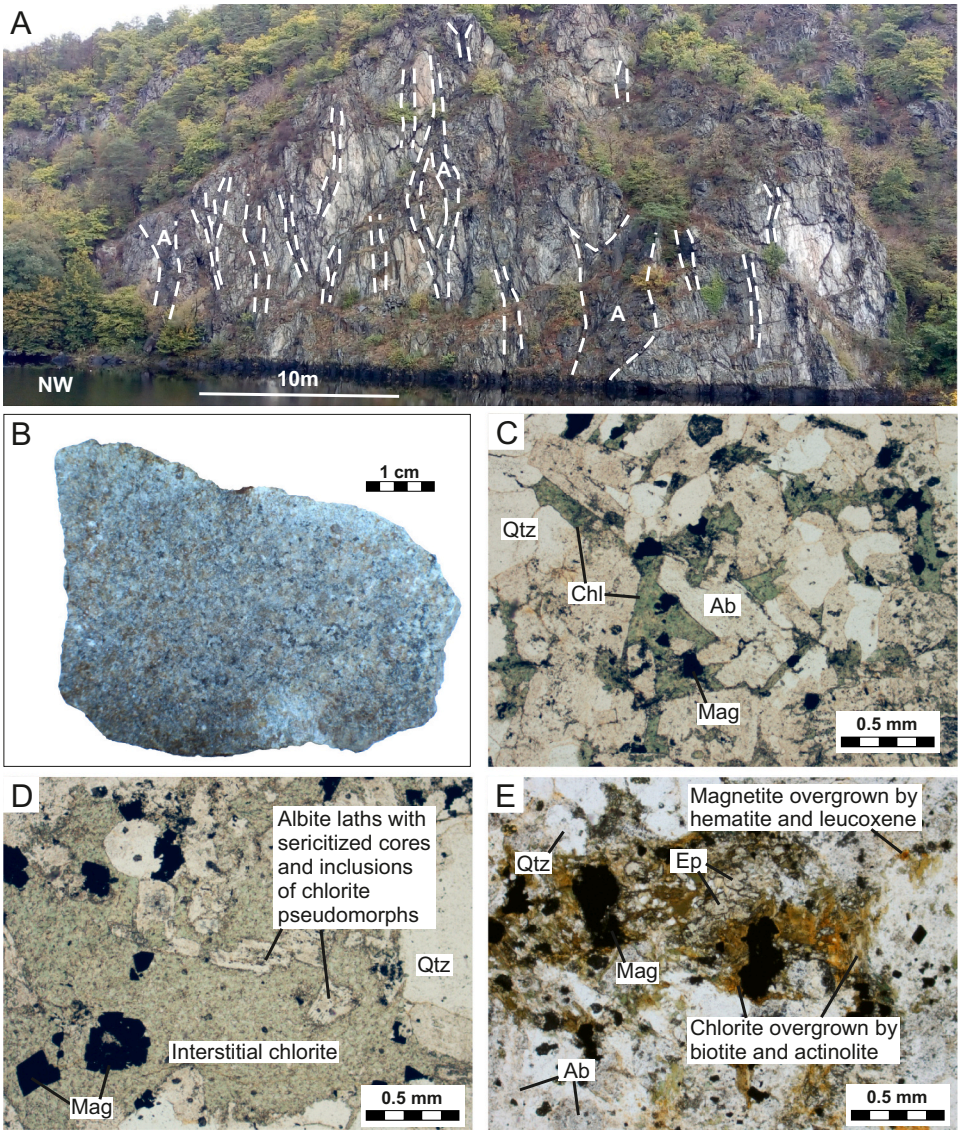


**Fig. 3.** (A) A trondhjemite intrusion intercalated with andesitic lava screens (dark rocks contoured by dashed lines) on the bank of the Vltava River near Třebenice village. (B) Rock piece of sample V-490 consisting of brown quartz, light grey albite and dark grey chlorite. (C, D) Photomicrographs of sample V-490 illustrating the trondhjemite petrography under a polarizing microscope, characterized by hypidiomorphic quartz and idiomorphic albite grains and chlorite filling the interstitial space. (E) A photomicrograph of sample VG-475 under a polarizing microscope, illustrating a metamorphic overprint in the DVC trondhjemite: local accumulations of epidote, biotite and actinolite replacing chlorite and hematite and leucoxene replacing magnetite; Qtz – quartz, Mag – magnetite, Chl – chlorite, Ab – albite, Ep – epidote. (For interpretation of the references to colour in this figure legend, the reader is referred to the web version of this article.)

resin (Triskem, France) for Sm and Nd extraction. Their isotopic compositions were measured on *Triton Plus* thermal ionization mass spectrometer (TIMS; Thermo); Sm and Nd contents were determined by isotopic dilution. For mass fractionation correction, $^{146}Nd/^{144}Nd = 0.7219$ and $^{147}Sm/^{152}Sm = 0.56081$ were used for Nd and Sm, respectively. The external reproducibility of Nd isotopic analyses was monitored by periodic measurements of the JNdi-1 solution with a $^{143}Nd/^{144}Nd$ ratio of 0.512100 ± 8 (2σ, $n = 24$). The accuracy of the whole protocol was monitored by measurements of BCR-2 reference material (USGS), which yielded concentrations of Nd = 28.6 ppm, Sm = 6.5 ppm, and the $^{143}Nd/^{144}Nd$ ratio of 0.512640 ± 12 in perfect agreement to previous results (Jochum and Nohl, 2008).

Hafnium isotopic data were collected at the joint laboratory of the IG CAS (sample preparation) and the Faculty of Science, Charles University (MC–ICP–MS analyses) following the protocol detailed in Ackerman et al. (2016). Approximately 150 mg of each sample were weighed, doped with appropriate amounts of $^{176}Lu$-$^{180}Hf$ spike and decomposed. Subsequently, Lu and Hf were isolated from the matrix by ion chromatography and measured using a Thermo *Neptune* MC–ICP–MS coupled with an Aridus II desolvating nebulizer. The in-house 50 ppb Hf isotopic solution, derived from PerkinElmer Inorganic Aqueous Single Hafnium Element Standard Solution, yielded a long-term $^{176}Hf/^{177}Hf$ value of 0.282132 ± 14, which is consistent with the long-term $^{176}Hf/^{177}Hf$ value of 0.282129 ± 7 obtained for the JMC-475 Hf isotopic solution. The accuracy of the method was monitored by measurements of BCR-2 reference material (USGS), which yielded concentrations of Lu = 0.52 ppm, Hf = 5.01 ppm and the isotopic ratio $^{176}Hf/^{177}Hf = 0.282840 \pm 4$, similar to previously published results (Jochum and Nohl, 2008).

### 3.4. Inverse geochemical modelling

In order to elucidate the petrogenetic process responsible for the formation of the DVC trondhjemite and LP IOAG in general, we performed inverse geochemical modelling using bulk-rock major and trace element compositions. The aim of this approach was to decipher the composition of the solid source for partial melting (PM) or parental melt for fractional crystallization (FC) considering the DVC trondhjemite composition as the final product ($C_L$).

For major element modelling, a mass balance equation with expressed $C_0$ was used:

$$C_0 = FC_L + (1 - F)C_S$$

where $C_0$ is the (unknown) concentration of a certain element in a solid source (applied for PM) or parental magma (applied for FC), $C_L$ is the

concentration of the element in a differentiated melt (DVC trondhjemite), and F is the degree of melting (PM) or the fraction of melt remaining (FC). The value of $C_S$ was calculated from the composition of fractionating minerals and their proportions (Supplementary Table 3a). Their compositions were taken from the literature (references provided in Supplementary Table 3a), while their proportions were inferred from experimental studies since there is no fractionation series preserved in the DVC.

For trace-element partial melting modelling, an inverted Shaw batch melting equation (Rollinson, 1993) with expressed $C_0$ was used:

$$C_0 = C_L[D + F(1 - D)]$$

where $C_0$ is the (unknown) concentration of a certain element in an unmolten source, $C_L$ is the concentration of the element in a differentiated melt (DVC trondhjemite), F is the degree of melting, and D is the bulk distribution coefficient for the residual phases.

For trace-element fractional crystallization modelling, we used an inverted Rayleigh equation (Rollinson, 1993) with expressed $C_0$:

$$C_0 = \frac{C_L}{F^{(D-1)}}$$

where $C_0$ is the (unknown) concentration of a certain element in parental melt, $C_L$ is the concentration of this element in differentiated melt (DVC trondhjemite), F is the fraction of melt remaining, and D is the bulk distribution coefficient for the crystallizing phases.

Two sets of mineral/melt distribution coefficients were compiled from the literature, one for a mafic and one for an intermediate–felsic environment (Supplementary Table 3b). The mafic set was used for PM and the mafic stage of FC, whereas the intermediate–felsic set was applied to intermediate–felsic FC. Trace element modelling employed the same mineral assemblages as major element modelling.

The results of inverse modelling were finally compared to selected intra-oceanic arc plutonic suites that include: (1) the Talkeetna gabbronorite–tonalite–trondhjemite representing lower/middle crust in the Alaskan Jurassic Talkeetna arc (Greene et al., 2006); (2) the Tanzawa gabbro–tonalite comprising lower/middle crust in the Miocene Izu–Bonin–Mariana arc (Kawate and Arima, 1998); (3) the Fiji trondhjemite from the evenly enriched (EE) suite of Marien et al. (2022) representing middle crust in the Eocene Fiji arc.

## 4. Results

### 4.1. Petrography and plagioclase compositions

Trondhjemite forms homogeneous intrusions with only subtle variations in mineralogy and geochemistry. The main intrusion is well exposed in the deeply incised valleys of the Vltava and Sázava rivers where continuous outcrops several km in length and up to ~100 m in height are exposed (Fig. 3A). The grey to pale pink rock (Fig. 3B) has well preserved fine- to medium-grained magmatic textures with weak subsolidus deformation. It is composed mainly of partly altered idiomorphic to hypidiomorphic plagioclase (40–55 vol%) of albitic composition [$An_{1-5}$; An = molar Ca/(Ca + Na + K) × 100] with some relics of oligoclase grains (~$An_{21}$) (Supplementary Table 2, Fig. 4A, B), quartz (30–40 vol%), pale green chlorite (10–15 vol%), epidote (2–5 vol %) and idiomorphic to allotriomorphic magnetite (~5 vol%) (Fig. 3C–E). Accessory minerals are represented by apatite, titanite, ilmenite, rutile and muscovite.

The originally zoned, up to ~3 mm long and mostly twinned skeletal plagioclase phenocrysts were completely homogenized into albite as documented by BSE (back-scattered electron), SEM (scanning electron

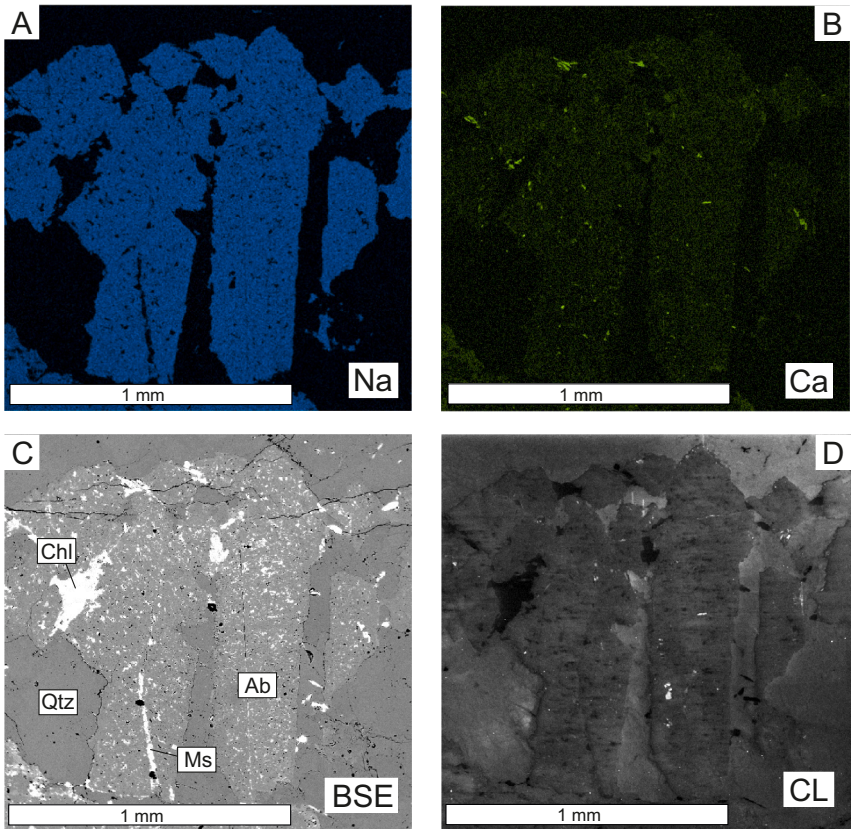


**Fig. 4.** Detailed petrography and microanalyses of plagioclase from the studied trondhjemites. (A, B) Compositional maps of Na and Ca, respectively, where plagioclase grains are dominated by albite, whereas Ca is accumulated in epidote, titanite and apatite. (C) A BSE image with highlighted minerals: Ab – albite, Qtz – quartz, Chl – chlorite and Ms. – muscovite (sericite). (D) A cathodoluminescence image showing the metamorphic/metasomatic texture of plagioclase grains.

microscope) and CL (cathodoluminescence) images (Fig. 4C, D). Chlorite is occasionally preserved as idiomorphic to hypidiomorphic columnar pseudomorphs after a primary Fe-Mg phase (most likely clinopyroxene or amphibole) but rather fills interstitial spaces between idiomorphic albite crystals incorporating thin idiomorphic laths of plagioclase and idiomorphic crystals of magnetite (Fig. 3D). Epidote occurs in the form of hypidiomorphic porphyroblasts forming accumulations or small veins. Fine-grained muscovite partly replaces albite, mainly along the contact with chlorite, and occurs along plagioclase cleavage plains and in originally calcic cores. The southeastern part of the trondhjemite body (closer to the contact with the CBPC) experienced higher degrees of metamorphism and deformation (Fig. 3E).

### 4.2. Bulk-rock major and trace element compositions

Bulk rock major and trace element data are listed in Table 1. In general, the trondhjemite displays very high $SiO_2$ and $Na_2O$ contents ranging from 72 to 77 wt% and 4.2–5.5 wt%, respectively. By contrast, $TiO_2$ (<0.5 wt%), CaO (<2.2 wt%) and $K_2O$ (<0.8 wt%) contents are very low, and $H_2O$ and $CO_2$ contents are <1.5 wt%. In the TAS discrimination diagram (Fig. 5A), the studied trondhjemites fall into the field of rhyolite; however, they resemble trondhjemite in composition when plotted in the Ab–An–Or discrimination diagram (O'Connor, 1965; Fig. 5B). The rocks follow the calc-alkaline series trend in the AFM and FeOt/MgO vs. $SiO_2$ diagrams (Fig. 6A, B) and generally belong to peraluminous, calcic and magnesian types based on the discrimination diagrams by Frost et al. (2001); Fig. 5C–E). The pillow lavas are of basaltic andesite to andesite composition with low $TiO_2$ concentrations and low $K_2O/Na_2O$ ratios. In both AFM and FeOt/MgO vs. $SiO_2$ diagrams, they plot near the boundary of tholeiitic and calc-alkaline trends.

The studied rocks show negative anomalies in HFSEs, such as Ti and P ($Ti_N/La_N$ = ~0.1–0.3, 0.3–0.45 for trondhjemites and pillow lavas, respectively, and $P_N/La_N$ = ~0.2–0.8; Fig. 5F), but a negative Nb anomaly is observed only in the trace element patterns of trondhjemites ($Nb_N/La_N$ = 0.4–0.9; Fig. 5F). Some fluid-mobile elements (e.g., Cs, Ba, U, K and Pb) are enriched relative to REEs and HFSEs in both rock types ($Ba_N/La_N$ = ~1.1–5.9, $U_N/La_N$ = ~2.3–5.4). Thorium, Rb and Sr, on the other hand, show negative anomalies ($Th_N/U_N$ = ~0.2–0.4, $Sr_N/La_N$ =

**Table 1**
Major and trace element compositions of the trondhjemites and pillow lavas from the Davle volcanic complex.

| Sample<br>rock type | 17CB23<br>pillow lava | 17CB01<br>pillow lava | V-469<br>trondhjemite | V-471<br>trondhjemite | VG-474<br>trondhjemite | VG-475<br>trondhjemite | V-648<br>trondhjemite | V-488<br>trondhjemite | V-490<br>trondhjemite |
|---|---|---|---|---|---|---|---|---|---|
| $SiO_2$ (wt%) | 53.3 | 56.4 | 73.4 | 75.2 | 75.8 | 74.6 | 73.8 | 73.1 | 72.0 |
| $TiO_2$ | 0.34 | 0.53 | 0.39 | 0.26 | 0.27 | 0.28 | 0.32 | 0.35 | 0.35 |
| $Al_2O_3$ | 17.1 | 15.6 | 14.6 | 12.8 | 12.5 | 13.3 | 12.5 | 13.0 | 12.6 |
| $Fe_2O_3$ | 2.3 | 0.41 | 0.93 | 2.0 | 1.6 | 2.4 | 2.1 | 1.3 | 5.6 |
| FeO | 7.0 | 8.3 | 1.3 | 1.0 | 0.5 | 0.8 | 1.8 | 1.4 | 0.2 |
| MnO | 0.20 | 0.18 | 0.03 | 0.03 | 0.03 | 0.05 | 0.08 | 0.04 | 0.04 |
| MgO | 5.1 | 4.6 | 1.0 | 1.1 | 0.76 | 0.37 | 0.80 | 1.6 | 1.4 |
| CaO | 8.0 | 2.9 | 1.5 | 1.0 | 2.0 | 2.2 | 0.3 | 1.5 | 0.37 |
| $Na_2O$ | 3.6 | 4.2 | 4.5 | 4.9 | 5.2 | 4.2 | 5.4 | 5.1 | 5.2 |
| $K_2O$ | 0.22 | 0.15 | 0.79 | 0.40 | 0.16 | 0.58 | 0.45 | 0.74 | 0.43 |
| $P_2O_5$ | 0.05 | 0.06 | 0.09 | 0.10 | 0.05 | 0.09 | 0.07 | 0.09 | 0.08 |
| $H_2O$- | 0.08 | 0.20 | 0.04 | 0.12 | 0.08 | 0.14 | 0.20 | 0.04 | 0.08 |
| $CO_2$ | < 0.01 | 0.71 | 0.11 | 0.16 | 0.10 | 0.09 | 0.13 | 0.40 | 0.13 |
| $H_2O$+ | 2.2 | 4.8 | 0.97 | 0.59 | 0.58 | 0.56 | 1.5 | 1.1 | 1.1 |
| S | < 0.01 | 0.07 | | | | | | | |
| Total | 99.5 | 99.1 | 99.6 | 99.8 | 99.5 | 99.6 | 99.5 | 99.7 | 99.7 |
| Sc (ppm) | 57 | 47 | 17 | 15 | 15 | 9 | 10 | 9 | 13 |
| V | 263 | 318 | 55 | 4.5 | 8 | 13 | 20 | 8 | 23 |
| Cr | 61 | 7.1 | <1 | 6.5 | 1.9 | 4.8 | 4.6 | 77 | 20 |
| Co | 33 | 23 | 3.0 | 1.6 | 0.9 | 3.1 | 5.3 | 3.3 | 4.6 |
| Ni | 26 | 13 | <1 | 4.7 | <1 | <1 | 2.7 | 38 | 6.3 |
| Cu | 103 | 111 | 5.3 | 5.3 | 6.8 | 5.8 | 3.8 | 0.8 | 0.4 |
| Zn | 87 | 83 | 20 | 25 | 14 | 25 | 35 | 21 | 28 |
| Rb | 2.2 | 4.2 | 7.3 | 4.9 | 1.9 | 11 | 5.8 | 8.2 | 4.7 |
| Sr | 170 | 57 | 64 | 97 | 93 | 115 | 147 | 54 | 81 |
| Y | 12 | 17 | 22 | 30 | 30 | 26 | 26 | 25 | 22 |
| Zr | 48 | 42 | 81 | 83 | 82 | 84 | 106 | 64 | 62 |
| Nb | 6.2 | 8.2 | 3.9 | 2.5 | 2.4 | 5.1 | 3.9 | 2.4 | 1.4 |
| Cs | 0.86 | 0.76 | 0.60 | 1.04 | 0.39 | 2.4 | 0.43 | 0.71 | 0.13 |
| Ba | 280 | 175 | 177 | 253 | 73 | 306 | 259 | 131 | 113 |
| La | 3.3 | 3.7 | 6.0 | 5.3 | 6.6 | 5.1 | 8.5 | 5.2 | 3.2 |
| Ce | 7.2 | 11.5 | 14 | 14 | 16 | 13 | 21 | 13 | 9.1 |
| Pr | 0.92 | 1.2 | 1.7 | 1.9 | 2.2 | 1.7 | 2.6 | 2.0 | 1.3 |
| Nd | 4.6 | 5.5 | 8.1 | 10 | 11 | 8.5 | 12 | 10 | 6.6 |
| Sm | 1.4 | 1.7 | 2.1 | 3.2 | 3.3 | 2.6 | 3.5 | 3.1 | 2.2 |
| Eu | 0.53 | 0.61 | 0.68 | 0.97 | 0.89 | 0.67 | 0.74 | 1.04 | 0.74 |
| Gd | 1.7 | 2.3 | 2.4 | 3.2 | 3.4 | 2.7 | 3.8 | 3.7 | 2.9 |
| Tb | 0.32 | 0.44 | 0.53 | 0.76 | 0.81 | 0.64 | 0.69 | 0.70 | 0.55 |
| Dy | 2.2 | 2.8 | 3.5 | 4.9 | 5.0 | 4.2 | 4.6 | 4.6 | 3.76 |
| Ho | 0.48 | 0.63 | 0.76 | 1.05 | 1.10 | 0.90 | 0.95 | 0.90 | 0.80 |
| Er | 1.4 | 1.9 | 2.6 | 3.6 | 3.8 | 3.2 | 3.0 | 3.1 | 2.58 |
| Tm | 0.22 | 0.28 | 0.40 | 0.51 | 0.51 | 0.45 | 0.43 | 0.40 | 0.34 |
| Yb | 1.3 | 1.9 | 2.6 | 3.6 | 3.5 | 3.0 | 3.3 | 3.1 | 2.65 |
| Lu | 0.20 | 0.30 | 0.41 | 0.54 | 0.56 | 0.44 | 0.46 | 0.43 | 0.37 |
| Hf | 1.7 | 1.4 | 2.6 | 2.7 | 2.6 | 2.6 | 3.4 | 2.3 | 2.1 |
| Ta | 1.7 | 0.63 | <0.5 | <0.5 | <0.5 | <0.5 | 0.28 | <0.20 | <0.20 |
| Pb | 2.8 | 1.7 | 1.4 | 2.8 | 1.1 | 1.2 | 1.3 | 3.5 | 1.7 |
| Th | 1.0 | 1.2 | 0.82 | 0.68 | 0.65 | 0.80 | 1.2 | 0.64 | 0.23 |
| U | 0.48 | 1.1 | 0.73 | 0.64 | 0.62 | 0.84 | 0.71 | 0.36 | 0.32 |

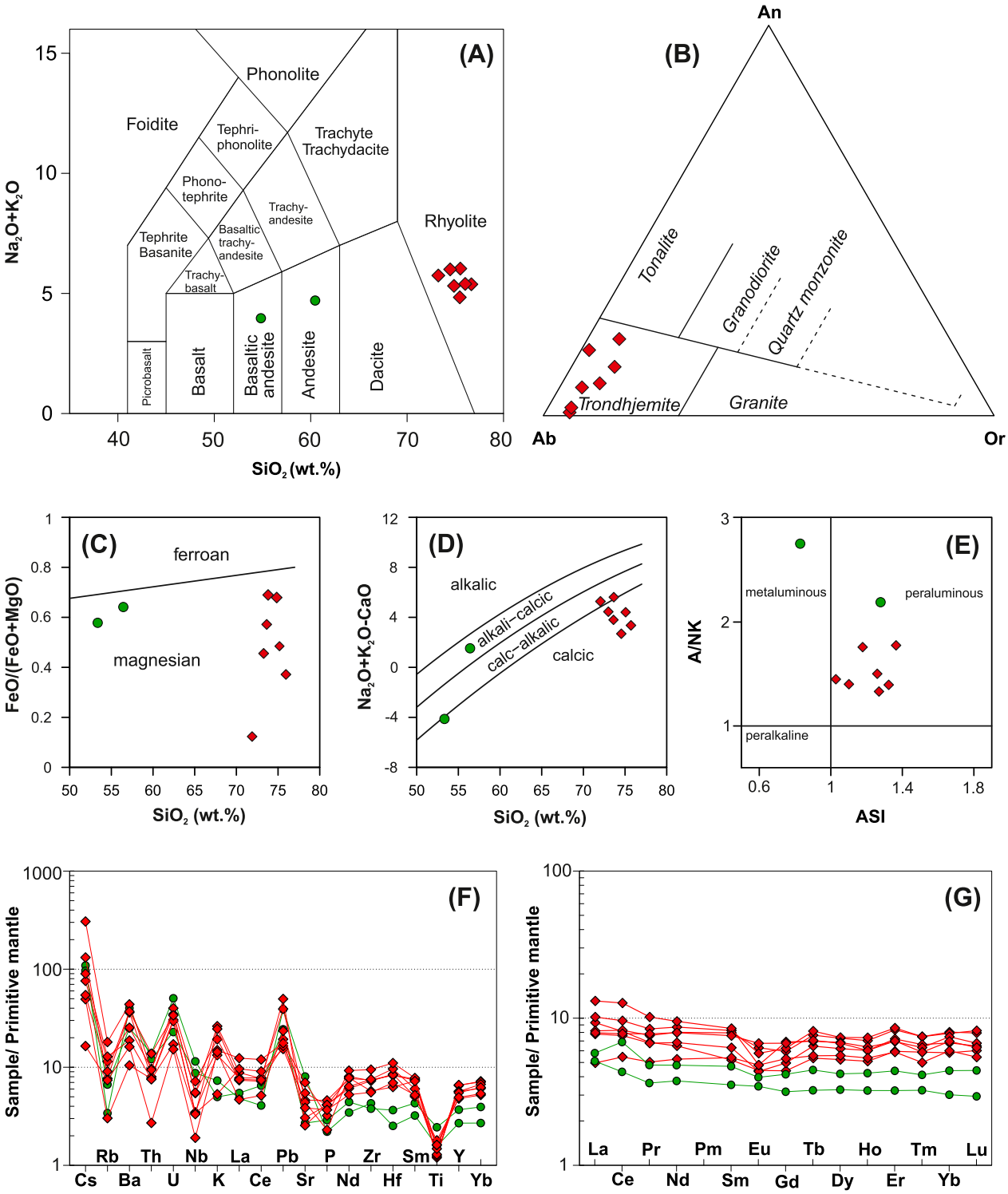


**Fig. 5.** (A) A TAS classification diagram after Le Bas et al. (1986). The analysed samples fall into the field of rhyolite, whereas the pillow lavas in the field of basaltic andesite and andesite. (B) Ab–An–Or classification diagram for granitic rocks after O'Connor (1965) with the analysed DVC samples falling into the field of trondhjemite. (C, D, E) Classification diagrams after Frost et al. (2001), characterizing the samples as magnesian, calcic and peraluminous. (F, G) Trace element and REE spider diagrams, respectively, normalized by primitive mantle (McDonough and Sun, 1995).

~0.3–0.8 and $Rb_N/Ba_N$ = ~0.2–0.7; Fig. 5F). Rare earth element contents normalized to primitive mantle (McDonough and Sun, 1995) of the trondhjemites and pillow lavas exhibit similar, rather flat patterns, slightly LREE-enriched and convex ($La_N/Yb_N$ = ~0.8–1.8; Dy/Dy* = ~0.8–1; Fig. 5G) with only slightly negative, if any, Eu anomaly (Eu/Eu* = ~0.8–1; Fig. 5G). The overall average concentration of REEs is higher in trondhjemites (~50 ppm) than in pillow lavas (~30 ppm). The concentrations of transitional metals compatible in the Earth's mantle, such as V, Cr, Ni and Zn, are widely scattered but mostly lower in the trondhjemites (V = 4–55 ppm, Cr ≤1–77 ppm, Ni ≤1–38 ppm, Zn = 14–35 ppm) and higher in the pillow lavas (V = 260–320 ppm, Cr = 7–60 ppm, Ni = 13–26 ppm, Zn = 83–88 ppm).

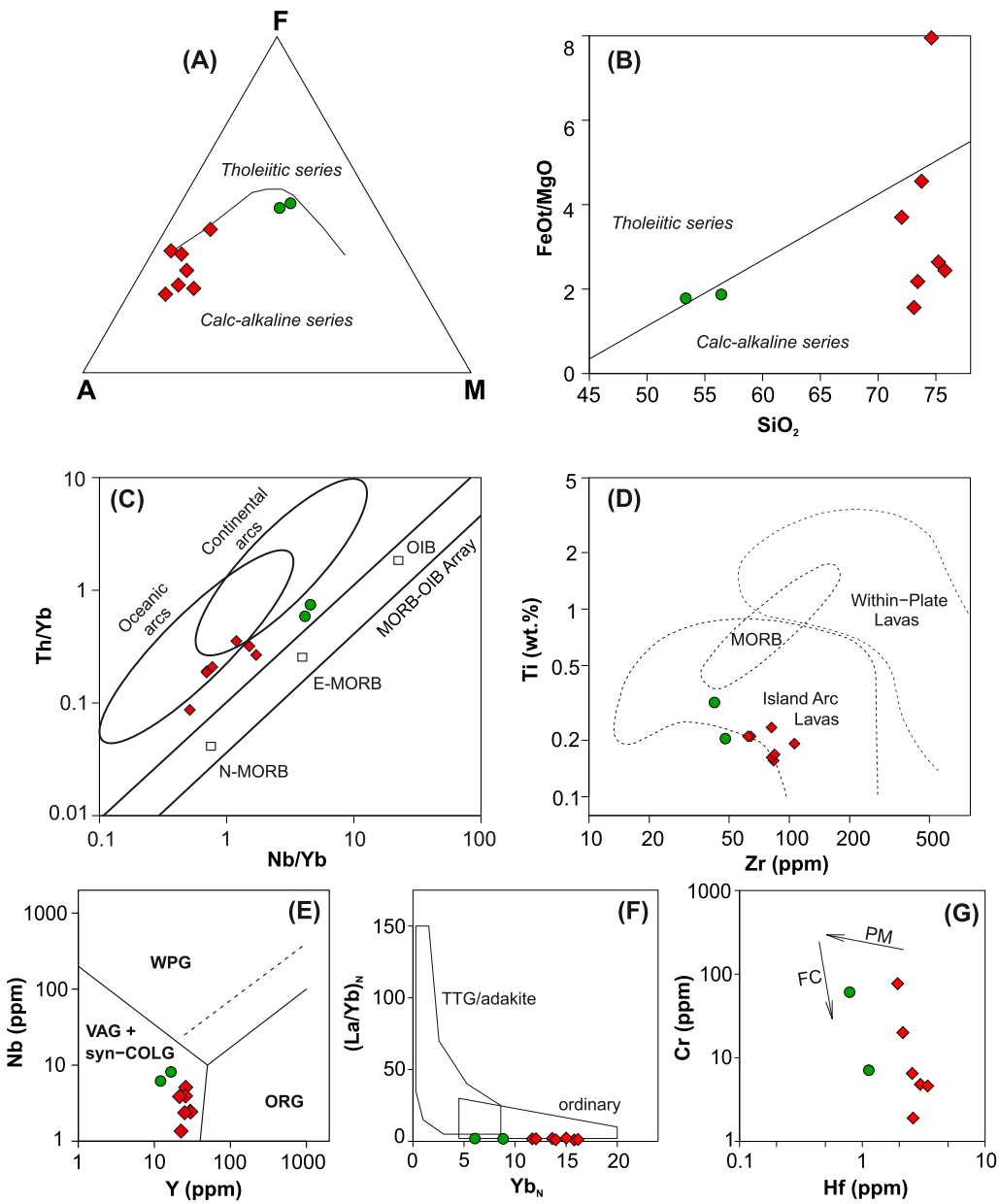


**Fig. 6.** (A, B) AFM and FeOt/MgO vs. $SiO_2$ diagrams, respectively, showing that the studied DVC trondhjemites follow a calc-alkaline trend. (C, D, E) Geotectonic discrimination diagrams after Pearce (2008), Pearce (1982) and Pearce et al. (1984), respectively, with the analysed samples resembling the composition of oceanic (island) arc rocks. (F) A diagram after Martin (1986), showing the affinity of the studied samples to ordinary rather than TTG/adakite magmas. (G) A Cr vs. Hf diagram (Cocherie, 1986) documenting that the studied trondhjemite follows a FC (fractional crystallization) trend rather than a PM (partial melting) trend.

### 4.3. Sm-Nd and Lu-Hf isotopic compositions

The Sm-Nd and Lu-Hf isotopic data are listed in Table 2. The initial isotopic compositions recalculated back to 600 Ma yielded $\varepsilon_{Nd}$ values from +6.0 to +8.7 and $\varepsilon_{Hf}$ values from +10.2 to +11.7 (Table 2) falling to the boundary between MORB (mid-ocean ridge basalt) and OIB (ocean island basalt) fields and close to the present-day DMM (depleted MORB mantle) reservoir with respect to $\varepsilon_{Hf}$ values (Fig. 7A). The pillow lavas show higher $\varepsilon_{Nd}$ values (+9.7 to +11.3) but lower $\varepsilon_{Hf}$ values (+8.4 to +8.6), falling further below the mantle array line, which might indicate remobilization of the elements by seawater during the extrusion on the ocean floor. The diagrams of isotopic composition vs.

**Table 2**
Nd and Hf isotopic compositions of the studied samples from the DVC.

| Sample | Rock Type | Nd (ppm) | Sm (ppm) | $^{147}Sm/^{144}Nd$ | $^{143}Nd/^{144}Nd$ | | $\varepsilon_{Nd}$ | Lu (ppm) | Hf (ppm) | $^{176}Lu/^{177}Hf$ | $^{176}Hf/^{177}Hf$ | | $\varepsilon_{Hf}$ |
|---|---|---|---|---|---|---|---|---|---|---|---|---|---|
| 17CB23 | pillow lava | 5 | 1.4 | 0.190 | 0.513192 | ± 11 | 11.3 | 0.20 | 0.78 | 0.036 | 0.283132 | ± 5 | 8.4 |
| 17CB01 | pillow lava | 6 | 1.9 | 0.192 | 0.513120 | ± 7 | 9.7 | 0.30 | 1.13 | 0.036 | 0.283136 | ± 5 | 8.6 |
| V-469 | trondhjemite | 8.2 | 2.2 | 0.138 | 0.512866 | ± 5 | 7.5 | | | | | | |
| V-471 | trondhjemite | 10 | 3.3 | 0.195 | 0.513075 | ± 12 | 8.7 | 0.57 | 2.55 | 0.031 | 0.283162 | ± 5 | 11.7 |
| VG-475 | trondhjemite | 8.6 | 2.7 | 0.159 | 0.512932 | ± 9 | 6.9 | 0.51 | 2.97 | 0.024 | 0.283041 | ± 6 | 10.2 |
| V-648 | trondhjemite | 13 | 3.4 | 0.176 | 0.512861 | ± 8 | 6.0 | | | | | | |
| V-488 | trondhjemite | 11 | 3.2 | 0.187 | 0.512974 | ± 22 | 7.3 | 0.53 | 1.94 | 0.038 | 0.283235 | ± 7 | 11.4 |
| V-490 | trondhjemite | 7.1 | 2.3 | 0.201 | 0.513084 | ± 12 | 8.4 | | | | | | |
| BCR-2 | reference | 29 | 6.5 | 0.138 | 0.512615 | ± 4 | | 0.52 | 5.01 | 0.014 | 0.282840 | ± 4 | |

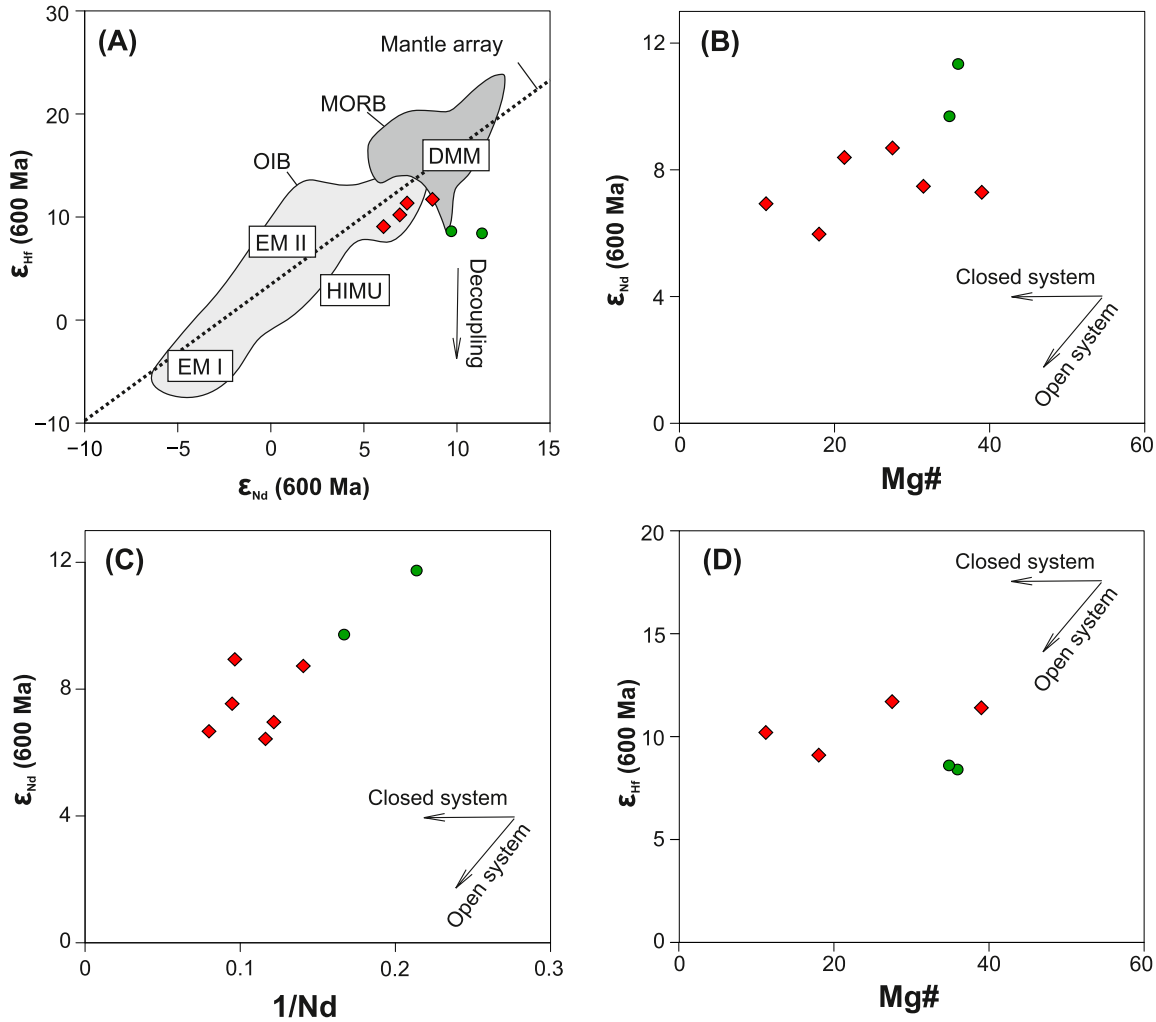


**Fig. 7.** (A) Results of isotopic analyses plotted in the $\varepsilon_{Nd}$ (i) vs. $\varepsilon_{Hf}$ (i) diagram. The DVC trondhjemite samples fall onto the boundary of Recent OIB and MORB fields with a minimal decoupling effect. In contrast, the pillow lavas were derived from a more depleted source but show a profound decoupling trend. The OIB and MORB fields were compiled from Patchett and Tatsumoto (1980), Salters (1996) and Salters and Hart (1991). Mantle array comes from Vervoort et al. (1999) whereas present-day DMM, EM I, EM II and HIMU reservoirs, plotted for a comparison, were compiled from Salters (1996) and Salters and Hart (1991). (B, C, D) $\varepsilon_{Nd}$ (i) vs. Mg#, $\varepsilon_{Nd}$ (i) vs. 1/Nd and $\varepsilon_{Hf}$ (i) vs. Mg# diagrams, respectively, showing a possible open system fractionation in a hypothetical magmatic evolution from pillow lavas to trondhjemites but a rather a closed system within the trondhjemite body.

independent fractionation indicator (Fig. 7B–D) point to a rather closed-system fractionation within the trondhjemite intrusion, but to possible open-system (mixing, assimilation) processes during a hypothetical magmatic evolution from pillow lavas to trondhjemites.

## 5. Discussion

### 5.1. Metasomatic/metamorphic overprint of the DVC trondhjemite

Whole-rock geochemical composition (Figs. 5–7) of the DVC trondhjemite might reflect magmatic as well as metamorphic/metasomatic processes (Moyen and Martin, 2012; Plümper and Putnis, 2009; Rollinson, 2009; Rong and Wang, 2016). Considering the observed petrographic features (Figs. 3–4), some metamorphic or metasomatic reactions must have been involved, including chloritization, epidotization, albitization and sericitization that collectively affected the primary mineral assemblage. For example, the overwhelming presence of albite that is completely homogenized with no preserved magmatic zoning (Fig. 4) and Ca contents that range only from $An_1$ to $An_5$ (Supplementary Table 2b) are typical attributes of subsolidus metasomatism (Plümper and Putnis, 2009; Rong and Wang, 2016). Albite grains preserve randomly distributed sericite (muscovite) inclusions (Fig. 4C) whereas epidote forms more localized accumulations. Chlorite, mostly filling interstitial spaces between albite and quartz grains, likely formed at the expense of other mafic minerals, e.g., clinopyroxene or amphibole (Fig. 3C). These mineral characteristics commonly accompany albitization (Plümper and Putnis, 2009; Rong and Wang, 2016), thereby supporting the subsolidus alteration hypothesis.

This alteration may have occurred (1) shortly after the trondhjemite subvolcanic intrusion during the Cadomian orogeny (Morávek and Röhlich, 1971; Röhlich, 1998), (2) in the course of Variscan regional metamorphism (Morávek and Röhlich, 1971), or (3) within Variscan thermal metamorphism related to the emplacement of the CBPC with joint hydrothermal fluid migration and Au mineralization (Zachariáš et al., 2013; Žák et al., 2014).

This metamorphism/metasomatism likely modified the budgets of fluid-mobile elements but the concentrations of fluid-immobile elements such as REEs, HFSEs, Y and Th, seem to be unaffected. This is demonstrated by the absence of correlation between fluid-mobile and fluid-immobile elements (see Supplementary figures). Yet, while REEs are immobile in hydrous fluids, they can be mobilized by $CO_2$-, halogen- and sulphate-rich fluids (e.g., Zheng et al., 2021). However, the DVC

trondhjemite displays very low $CO_2$ concentrations (Table 1), and the inferred Variscan mineralization is also dominated by $H_2O$-rich fluids with only a minor $CO_2$ admixture (Zachariáš et al., 2013).

To conclude, the DVC trondhjemite was affected by some degree of metamorphism and/or metasomatism. Although these processes cannot be characterized in detail, we do not consider them to be responsible for a significant modification of the fluid-immobile element budgets. Therefore, the fluid-immobile elements such as REEs, Th, Nb, P, Zr, Hf, Ti and Y can be used for the evaluation of magmatic processes using geochemical modelling.

### 5.2. Geotectonic setting of the DVC trondhjemite

The DVC trondhjemite exhibits several geochemical features indicative of its formation in a subduction-related geotectonic setting, as suggested for the whole DVC by previous studies (e.g., Ackerman et al., 2019; Ackerman et al., 2021; Hajná et al., 2011; Křibek et al., 2000; Sláma et al., 2008; Waldhauserová, 1984). Notably, it follows a calc-alkaline trend in the AFM and FeOt/MgO vs. $SiO_2$ diagrams (Fig. 6A, B), and exhibits characteristic trace element signatures typically ascribed to subduction-related settings, such as an enrichment in large-ion lithophile elements (LILE) and a depletion in HFSEs (e.g., Kelemen et al., 2003; Fig. 5F). Indeed, the samples plot to the island-arc field in several geotectonic discrimination diagrams (Fig. 6C–E).

On the other hand, the only mildly LREE-enriched to flat REE patterns ($La_N/Yb_N = 0.9–1.9$), low Sr/Y ratios (< 5) and low concentrations of $K_2O$ and Th contrast with those of typical subduction-related volcanic and plutonic rocks formed by high-pressure fractionation/melting with garnet-bearing residua/restites (e.g., Moyen, 2009; Figs. 6F, 8A–B, E–F) or rocks which underwent assimilation of evolved crust (e.g., D'Souza et al., 2016). Similarly, the flat REE patterns of the DVC trondhjemite differ from the LREE-depleted patterns of oceanic plagiogranites (Freund et al., 2014; Rollinson, 2009; Fig. 8A–B, E–F).

By contrast, the trace element signatures of the DVC trondhjemite resemble those reported for juvenile intra-oceanic arc igneous rocks formed at low pressures (Greene et al., 2006; Kawate and Arima, 1998; Leat et al., 2007; Fig. 8C–F), herein referred to as "low-pressure intra-oceanic arc granitoids" or "LP IOAG". The lower Th contents and higher Nb contents, resulting in the lower Th/Nb ratios of the DVC trondhjemite, pose the only encountered deviation from the composition of the LP IOAG (Fig. 8F). This may be explained by a different element input from the subducting plate.

At the same time, the significantly radiogenic Nd-Hf isotopic signature ($\varepsilon_{Nd} = +6.0$ to $+8.7$ and $\varepsilon_{Hf} = +10.2$ to $+11.7$; Fig. 7A–D) combined with the low contents of Th clearly indicate a juvenile igneous source of the DVC trondhjemite. The slightly enriched Nd-Hf characteristics compared to DMM can be acquired either by an enriched character of the mantle wedge (either due to metasomatism by a subduction-related fluid or by a mantle plume (Ackerman et al., 2019; Salters, 1996), or by minor assimilation of older crust. To sum up, an intra-oceanic island-arc geotectonic setting of the DVC trondhjemite shows the best fit with the acquired geochemical data.

### 5.3. Geotectonic setting of the DVC pillow lavas

Compared to the DVC trondhjemite, the pillow lavas resemble magmas from a less evolved arc. For instance, they are characterized by higher FeOt/MgO ratios relative to their $SiO_2$ and alkali contents, transitional between the tholeiitic and calc-alkaline trends (Fig. 6A, B). They do not show a negative Nb anomaly ($Nb_N/La_N = \sim1.8–2.1$) and their isotopic signature points to their derivation from highly depleted MORB-like mantle (Fig. 7A–C).

Nonetheless, their geochemical composition does not match MORB (either N-MORB or E-MORB) characteristics completely. For example, they show negative Ti and P anomalies ($Ti_N/La_N = \sim0.3–0.45$, $P_N/La_N = \sim0.2–0.8$; Fig. 5F), elevated LREE and Th contents but lower HREE and Y contents. Altogether, these features imply that the pillow lavas plot to the field of volcanic arcs in the diagnostic geotectonic diagrams (Fig. 6D–E).

To conclude, the pillow lavas were likely formed in less evolved arc conditions prior to the trondhjemite intrusion. Therefore, it is unlikely that they represent a possible parental melt for the studied trondhjemite.

### 5.4. Petrogenesis of the DVC trondhjemite

It has been suggested that low-pressure intra-oceanic arc granitoids (LP IOAG) may form large portions of island-arc middle crust worldwide (DeBari and Greene, 2011; Greene et al., 2006; Jagoutz and Kelemen, 2015). Such rocks have been found in the middle crust of several exposed ancient island arcs (DeBari and Greene, 2011; D'Souza et al., 2016; Greene et al., 2006; Kawate and Arima, 1998) and are suspected to be present also in modern island arcs since seismic imaging revealed low-velocity (6.0–6.5 $km \cdot s^{-1}$) P-wave layers in their middle crust (Calvert, 2011; DeBari and Greene, 2011; Leat et al., 2007). Therefore, LP IOAG provide key information for a better understanding of the processes of siliceous crust formation from juvenile (isotopically depleted) sources and therefore contribute to the long-lasting and vigorous debate on the dynamics of Earth's crust growth.

It is generally assumed that the formation of LP IOAG can be attributed to two contrasting processes: (1) partial melting (PM) of mafic lower crust represented by gabbro or amphibolite (Beard, 1995; Brophy, 2008; Chen et al., 2019; DeBari and Greene, 2011; Jagoutz and Kelemen, 2015; Rollinson, 2009), or (2) fractional crystallization (FC) of the parental mafic/intermediate magma. Two quite robust methods for their discrimination, applicable to intra-oceanic arcs, have been proposed: (1) Brophy (2008) suggested the use of La vs. $SiO_2$ and Yb vs. $SiO_2$ variation diagrams. Unfortunately, the variation in $SiO_2$ contents of the studied trondhjemites is very limited and the observed trends cannot be interpreted with confidence. (2) Cocherie (1986) developed trace element log-log diagrams to distinguish between the two mentioned processes. The wide variation in the contents of highly compatible element (e.g., Cr) together with the narrow scatter in the contents of incompatible element (e.g., Hf, Fig. 6G) argue for fractional crystallization at least in the final stages of magmatic evolution of the DVC trondhjemite.

### 5.5. Deciphering the sources of the DVC trondhjemite through inverse geochemical modelling

#### 5.5.1. Partial melting

Evidence for partial melting of lower/middle island-arc crust (i.e., migmatite) has been regularly found on exposed island arcs (DeBari and Greene, 2011). Several experimental studies on low pressure PM (garnet-free residue) attempted to explain the nature of sources parental for arc-related magmas (Beard and Lofgren, 1991; Nakajima and Arima, 1998; Rapp and Watson, 1995). In general, these investigations focused on PM at 0.1–1 GPa and 800–1075 °C using metabasalts and metabasaltic andesites as starting materials.

Here, plagioclase is the most abundant residual phase, often representing >50% of the residual minerals (Beard and Lofgren, 1991), dominating over clinopyroxene, orthopyroxene, amphibole, magnetite, ilmenite and in some cases olivine (Beard and Lofgren, 1991; Nakajima and Arima, 1998; Rapp and Watson, 1995). However, the proportion of mafic minerals (pyroxenes vs. amphibole) is strongly dependent on the presence of water assisting at the melting: amphibole is not stable during dehydration melting, so clinopyroxene with smaller amounts of orthopyroxene prevail regardless of the pressure. In water-excess melting, however, amphibole becomes stable and prevails over both pyroxenes (Beard and Lofgren, 1991). Considering these experimental data, we employed the inverse partial batch melting model. A residual mineral assemblage consisting of 55% plagioclase (An = 90), 25% clinopyroxene, 10% orthopyroxene, 8.6% magnetite and 1.4% ilmenite was used for dehydration melting, while an assemblage of 50% plagioclase (An =

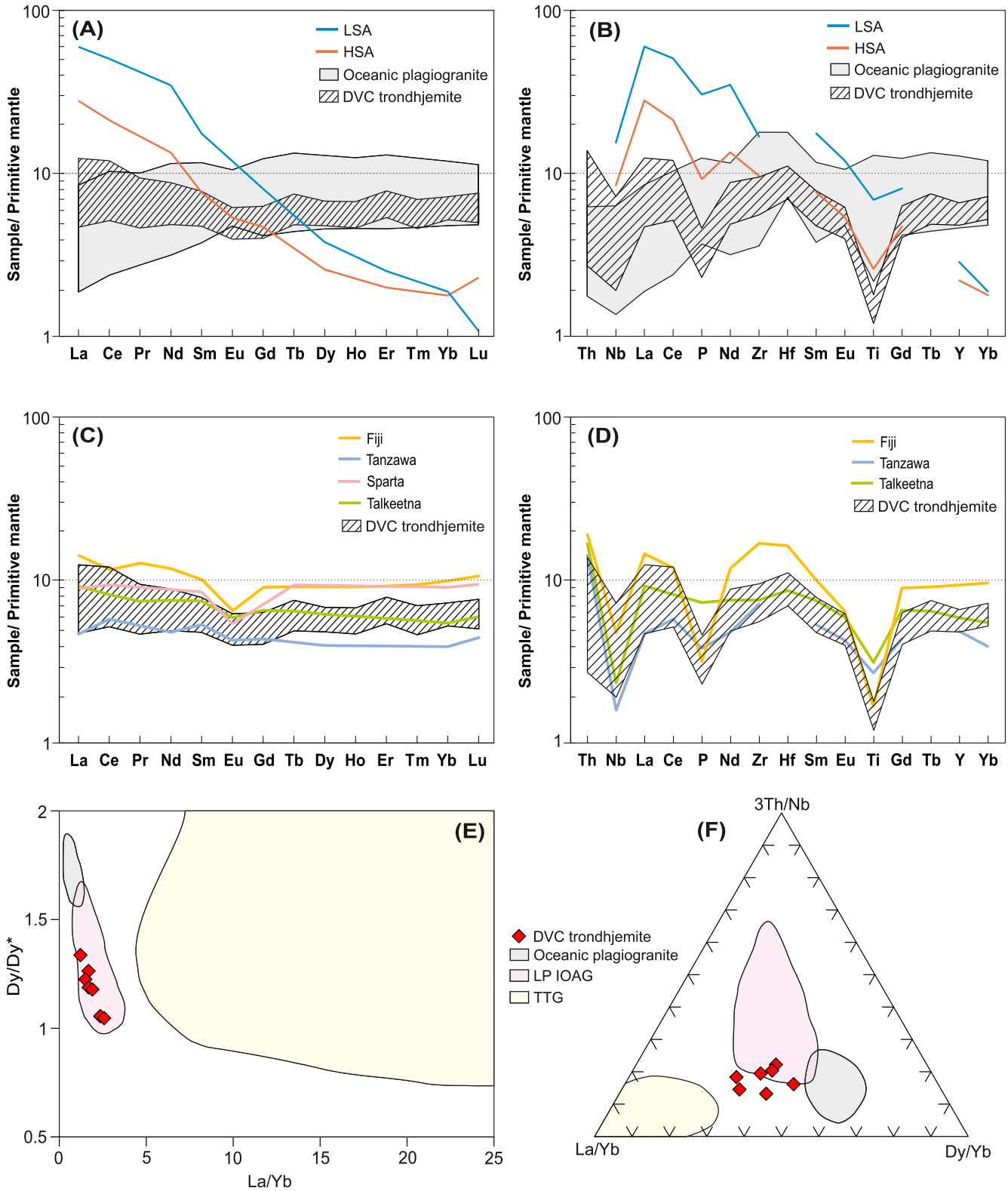


**Fig. 8.** (A, B) A comparison of the studied trondhjemite with the oceanic plagiogranite range – compiled from Troodos main group (Freund et al., 2014) and Semail Rajmi group (Rollinson, 2009), and with average low-silica adakites (LSA) and high-silica adakites (HSA) (Martin et al., 2005) on a primitive mantle-normalized (McDonough and Sun, 1995) REE and immobile trace element spider plots. (C, D) A comparison of the DVC trondhjemite with different "low-pressure island-arc granitoids – LP IOAG" on primitive mantle-normalized (McDonough and Sun, 1995) spider plots. References: Fiji (Marien et al., 2022), Tanzawa (Kawate and Arima, 1998), Sparta (Phelps and Avé Lallemant, 1980), Talkeetna (Greene et al., 2006). (E, F) Diagrams showing different immobile trace element ratios of TTG (references given in Supplementary Table 5), LP IOAG – compiled from Greene et al. (2006), Kawate and Arima (1998) and Marien et al. (2022), and oceanic plagiogranites – compiled from Freund et al. (2014) and Rollinson (2009).

90), 40% amphibole, 8.6% magnetite and 1.4% ilmenite was used for water-excess melting.

Based on the major element mass balance calculation, the model predicts that ~20–40% partial melting (either water-excess or dehydration) can account for the highly siliceous composition of the DVC trondhjemite. Most of the modelled major element trends were found to correspond with those reported from the better exposed intra-oceanic arcs (Greene et al., 2006; Kawate and Arima, 1998; Kelemen et al., 2003; Fig. 9A–G). However, some were found to be significantly different. For example, the model lacks $P_2O_5$ enrichment at intermediate

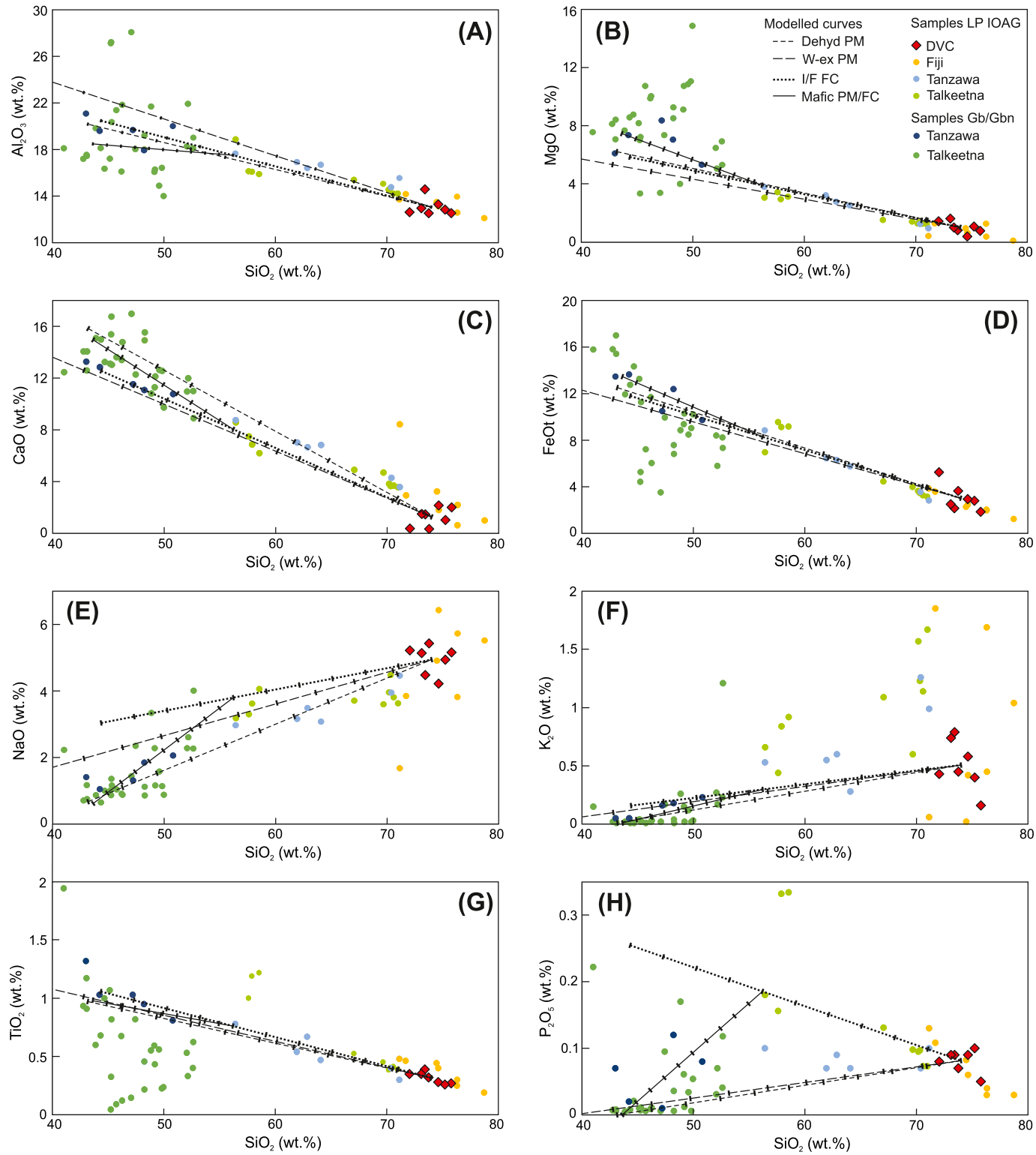


**Fig. 9.** Results of major element inverse geochemical modelling displayed in $SiO_2$ vs. selected major elements binary diagrams: Dehyd PM – dehydration partial melting, W-ex PM – water-excess partial melting, I/F FC – intermediate to felsic fractional crystallization, Mafic PM/FC – mafic stage partial melting or fractional crystallization; see text for details. The bars on the modelled curves represent 10% step (F = 0.1). The modelled trends are compared to samples (LP IOAG and Gb/Gbn – gabbros and gabbronorites) from better exposed island arcs: Fiji (Marien et al., 2022), Tanzawa (Kawate and Arima, 1998) and Talkeetna (Greene et al., 2006).

compositions due to the absence of apatite in the fractionation assemblage (Fig. 9H).

Bigger differences between the dehydration and water-excess melting models can be recognized in trace element, especially REE patterns. Due to the higher compatibility of MREEs and HREEs in amphibole, the REE pattern of the source modelled by water-excess melting shifted towards a concave curve with higher Dy/Yb, Dy/Dy* and lower La/Yb ratios (Figs. 10–11). On the other hand, REE patterns of the source for dehydration melting tended to maintain the shape and slope of the melt, resulting in minimum changes in the Dy/Yb, Dy/Dy* and La/Yb ratios (Figs. 10–11). Both models predicted lower concentrations of REEs as well as all other incompatible elements in the source compared to the melt since the mineral/melt distribution coefficient ($K_D$) values of these elements in the modelled minerals in mafic environment were < 1. Yet, the dehydration melting model provided lower overall concentrations of REE and incompatible trace elements in the source than the water-excess model because amphibole, which is present only in the water-excess model, has a higher $K_D$ value than pyroxenes or plagioclase. Both models predicted higher Eu/Eu* in the source since plagioclase was an abundant residual phase in both melting types. Nevertheless, none of the partial melting models generated the LREE-depleted curves observed in lower-crustal gabbros and gabbronorites from the exposed intra-oceanic arcs (Greene et al., 2006; Kawate and Arima, 1998; Fig. 11B, E). We therefore conclude that partial melting of lower-crustal gabbros and gabbronorites and similar rock types, generating directly highly siliceous (<70 wt% $SiO_2$) magmas, is an unlikely process for the DVC trondhjemite formation.

### 5.5.2. Fractional crystallization

In the exposed ancient intra-oceanic island arcs, mafic gabbro cumulates are present within the lower/middle crust (Beard, 1995; DeBari and Greene, 2011; Greene et al., 2006). These rocks, consisting of plagioclase, clinopyroxene, orthopyroxene, Mg-Al spinel, Fe-Ti oxide but also minor amphibole and garnet, were interpreted to form by crystal accumulation of minerals from already fractionated mantle-derived magmas (DeBari and Greene, 2011; Greene et al., 2006). The residual melt follows the fractionation path and eventually crystallizes in the form of either plutonic or volcanic intermediate–felsic rocks (Greene et al., 2006).

Experimental studies on fractional crystallization (FC) of hydrous arc magmas at pressures from 0.4 to 0.9 GPa provide evidence that the main phases which crystallized from the melt at a decreasing temperature from ~1200 to 700 °C are represented by olivine, clinopyroxene + orthopyroxene, plagioclase + amphibole + spinel/magnetite (Blatter et al., 2013; Nandedkar et al., 2014). Their proportions are strongly dependent on the basicity of the melt. Olivine crystallizes only from basaltic magmas ($SiO_2$ < ~50 wt%) while clinopyroxene (with a small amount of orthopyroxene) is the dominant crystallizing phase from melts of basaltic composition but strongly diminishes towards more acidic magmas. At intermediate to felsic melt compositions, fractionation is governed by crystallization of plagioclase and amphibole accompanied by minor magnetite, ilmenite and trace apatite. Other trace phases such as Cr-spinel, Al-spinel or biotite may be also present but are omitted from our models.

The above experimental data were taken as a basis for inverse FC modelling of intermediate–felsic magma. The crystallizing phases were set as follows: 50% plagioclase (An = 61), 30% amphibole, 10% clinopyroxene, 8% magnetite, 1.4% ilmenite and 0.6% apatite.

Major element mass balance models were generally found to follow the trends of the tonalite–trondhjemite suites of the Talkeetna and the Izu–Bonin–Mariana (Tanzawa tonalite) arcs (Fig. 9). Trace elements are characterized by an overall depletion in the parental magma relative to the final melt (DVC trondhjemite) except for the MREEs and Y, which are compatible in amphibole and therefore not depleted in the parental magma (Figs. 10, 12A, B, D, E). Amphibole fractionation is illustrated by decreasing La/Yb and increasing Dy/Yb and Dy/Dy* ratios (Fig. 10)

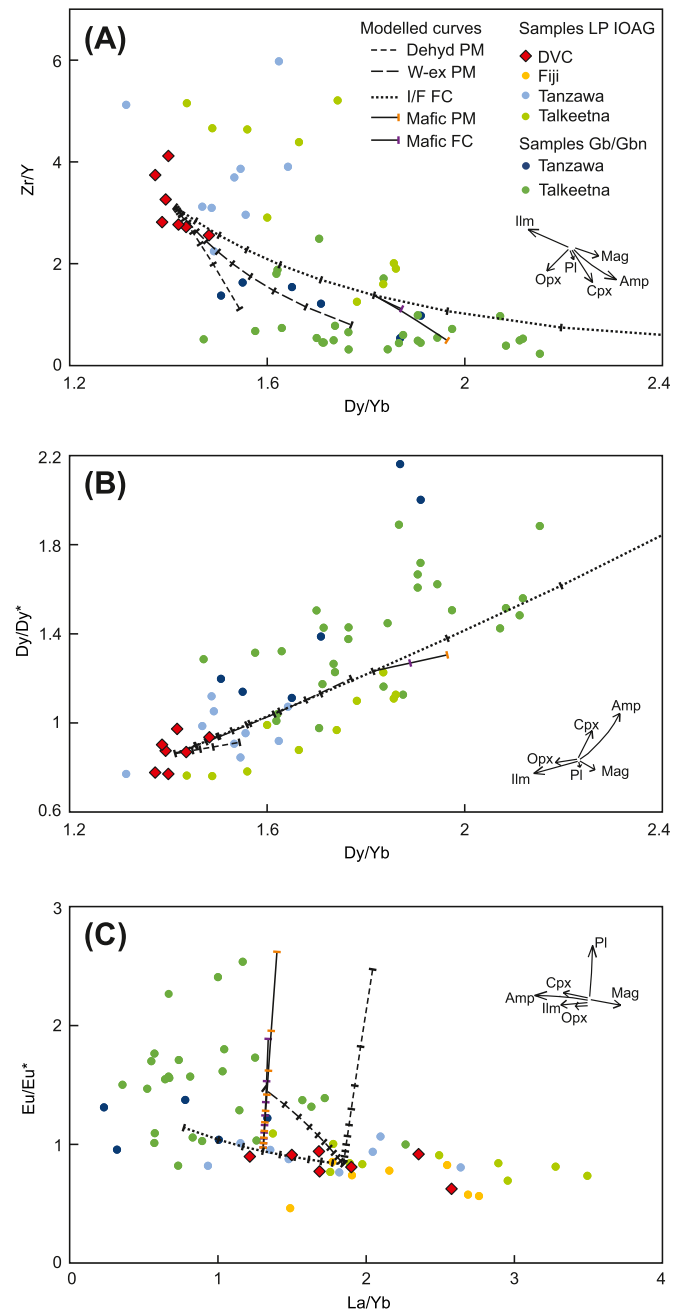


**Fig. 10.** Results of trace element inverse geochemical modelling displayed in binary diagrams: Dehyd PM – dehydration partial melting, W-ex PM – water-excess partial melting, I/F FC – intermediate to felsic fractional crystallization, Mafic PM – mafic stage partial melting, Mafic FC – mafic stage fractional crystallization; see text for details. The bars on the modelled curves represent 10% step (F = 0.1); only for mafic PM and mafic FC in the panels A and B, there is only one bar plotted standing for 100% (F = 1) and 90% (F=0.9), respectively. The modelled trends are compared to samples (LP IOAG and Gb/Gbn – gabbros and gabbronorites) from better exposed island arcs: Fiji (Marien et al., 2022), Tanzawa (Kawate and Arima, 1998) and Talkeetna (Greene et al., 2006). Also, inverse trends of mineral fractionation are shown: Ilm – ilmenite, Mag – magnetite, Amp – amphibole, Pl – plagioclase, Cpx – clinopyroxene, Opx – orthopyroxene.

towards the parental magma composition. The Eu anomaly was found to shift very reluctantly towards positive values in the parental magma (Fig. 10C) although plagioclase constituted 50% of the crystallizing phases in the model. This can be best explained by the lower $K_D$ of Eu in amphibole compared to those of other MREEs especially in felsic

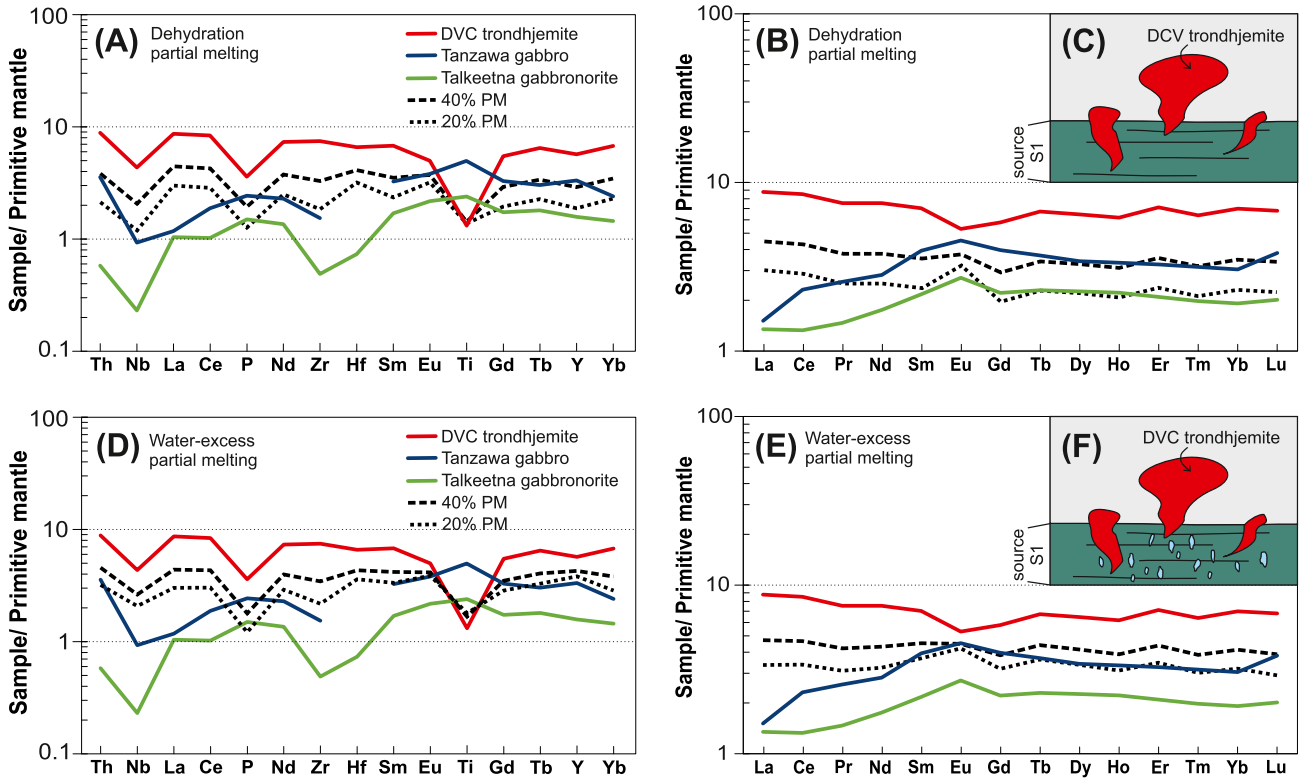


**Fig. 11.** Primitive mantle-normalized (McDonough and Sun, 1995) spider plots showing the results of trace element inverse geochemical modelling for dehydration PM (A, B) and for water-excess PM (D, E). The modelled curves do not match the general trends of exposed lower crustal gabbros and gabbronorites demonstrated by average values from the Tanzawa gabbros (Kawate and Arima, 1998) and Talkeetna gabbronorites (Greene et al., 2006). The partial melting process is illustrated by the attached cartoons (C, F).

magmas (reverse to plagioclase), which would diminish a positive Eu anomaly in the parental melt. The modelled bulk trace element concentrations are still much higher than the averages for basic plutonic rocks reported from exposed intra-oceanic arcs (Greene et al., 2006; Kawate and Arima, 1998) but fit quite well to the patterns of the most primitive rocks of the tonalite suites from these arcs (Fig. 12A, B, D, E). Taking this into account together with the observed FC trends in the Cr-Hf diagram (Fig. 6G) and the results of our major element modelling (Fig. 9), we suggest that the DVC trondhjemite could have formed from a parental tonalitic melt through FC.

#### 5.5.3. *A source for a primitive tonalitic melt*

Approximately 60% FC (F = 0.4) is required to reach the chemical composition of the most primitive LP IOAG (~55 wt% $SiO_2$) through inverse geochemical modelling (Fig. 9). To determine the source for this parental tonalitic melt, we performed inverse geochemical modelling of dehydration PM and FC, setting the tonalitic melt modelled in the previous step as a daughter magma ($C_L$, L1 in Fig. 12C, F, I). The same mineral assemblage of the restite (PM) and the cumulus (FC) was used: 50% plagioclase, 25% clinopyroxene, 15% orthopyroxene, 8.6% magnetite and 1.4% ilmenite.

The modelled trends of major and immobile trace elements coincide with the composition of at least some of the very heterogeneous lower-crustal gabbro/gabbronorite samples (Greene et al., 2006; Kawate and Arima, 1998; Figs. 9, 10, 12). Greene et al. (2006) successfully modelled REE patterns of the evolving gabbroic-tonalitic melt from the Talkeetna arc through three-stage FC whereas Kawate and Arima (1998) modelled the composition of the Tanzawa gabbro as a mixture of a partial melt with a co-genetic restite. The compositional heterogeneity probably arises from the variety of the cumulus or restite phases and their mixing proportion with the evolved melt. While modelling of such complex processes is beyond the scope of this paper, we note that our inverse model demonstrates some general trends, such as the nearly constant La/Yb, Dy/Yb and Zr/Y ratios, and also the rapidly increasing Eu/Eu* ratio towards more mafic magmas (Fig. 10).

### 5.6. *Implications for crustal growth*

It has been assumed that the post-Archean continental crust is produced mainly by accretion of island arcs to the continents at convergent plate boundaries (e.g., Stern and Scholl, 2010). Therefore, the understanding of the island-arc crust formation is crucial to reveal the triggers and tempos of crustal growth. In this respect, intra-oceanic island arcs, where juvenile melts with a negligible assimilation of matured crust are generated, represent a natural laboratory for the study of the prime principle of crustal growth. While the melts that reach the surface are dominantly mafic (Gill, 1981), seismic profiles across active intra-oceanic arcs reveal that the middle crust is rather intermediate to felsic in its composition (Calvert, 2011), hence probably composed mainly of tonalitic–trondhjemitic plutons (DeBari and Greene, 2011). As the middle crust is only rarely exposed in modern island arcs, we are reliant on the preserved ancient intra-oceanic arcs.

Since any mafic precursors of the tonalitic–trondhjemitic plutons are commonly missing in surface exposures, which is also the case of the DVC trondhjemite, our approach was to use inverted equations for geochemical modelling to calculate the source composition from the known final melt composition. Based on the modelling results and a comparison of the DVC trondhjemite with LP IOAG from the well-exposed Talkeetna (Greene et al., 2006) and Izu–Bonin–Mariana (Tanzawa; Kawate and Arima, 1998) arcs, we argue that the LP IOAG can be produced by a combination of fractional crystallization or partial melting of mafic precursors followed by fractional crystallization. This process can collectively account for the compositional variety observed in the island-arc tonalite–trondhjemite suites. Our study also

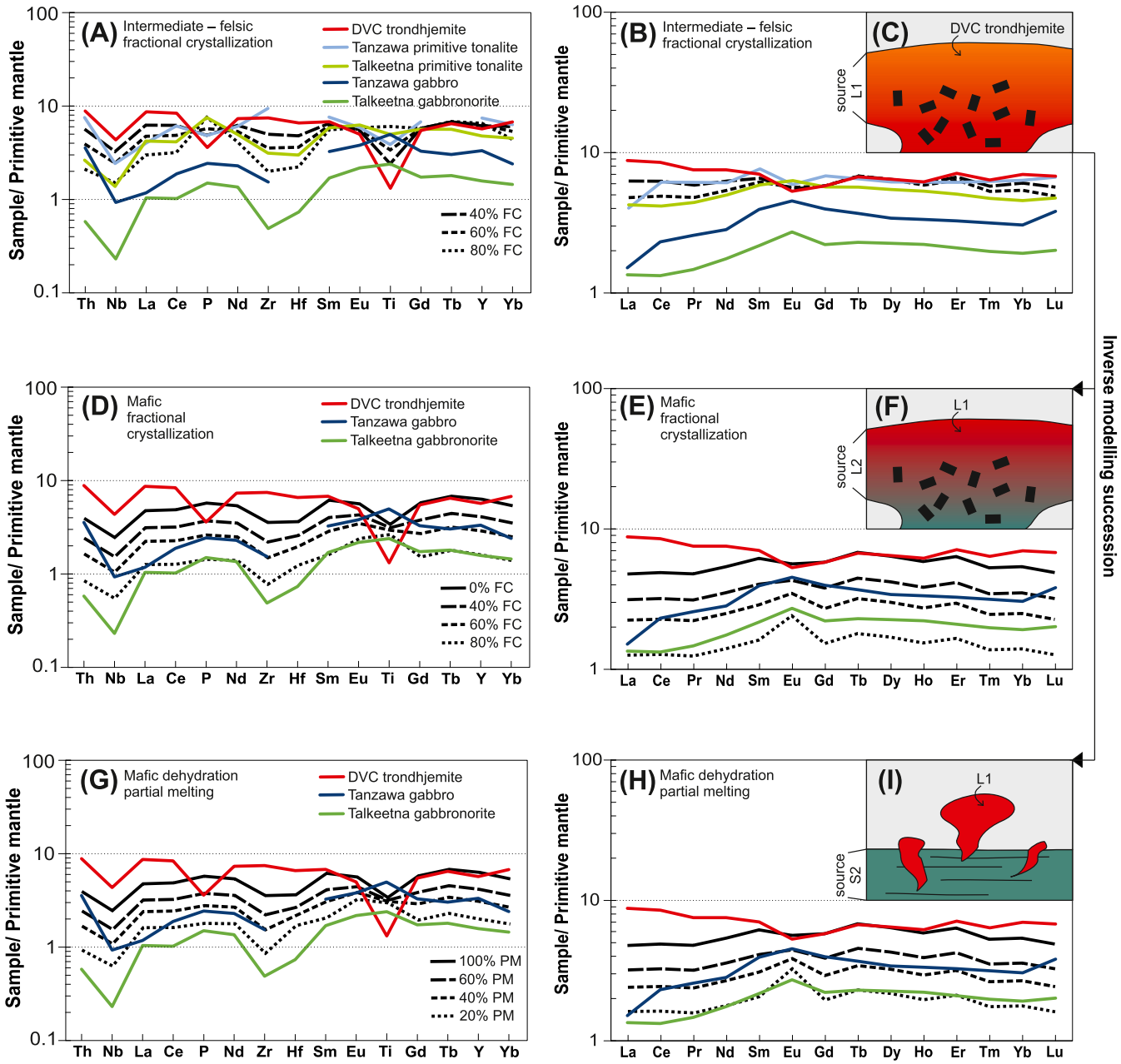


**Fig. 12.** Primitive mantle-normalized (McDonough and Sun, 1995) spider plots showing the results of trace element inverse geochemical modelling for intermediate to felsic FC (A, B) and subsequent mafic FC (D, E) and dehydration PM (G, H). The modelled curves of the intermediate to felsic FC approximately coincide with the most primitive tonalitic compositions from better exposed island arcs: Tanzawa – sample AZ-5 of Kawate and Arima (1998), and Talkeetna – sample 0720A4 of Greene et al. (2006). The results of the 60% FC were subsequently used as the final melt (L1) for the determination of its source through FC (D, E) or PM (G, H). The patterns modelled in this step approximately fit the general trends of exposed lower crustal gabbros and gabbronorites demonstrated by average values from the Tanzawa gabbros (Kawate and Arima, 1998) and Talkeetna gabbronorites (Greene et al., 2006). To clarify the petrogenetic process, cartoons showing the intermediate to felsic FC (C), mafic FC (F) and mafic PM (I) are attached.

demonstrates that no major input of subduction-derived melts or assimilation of older crust are required to produce large volumes of intermediate–felsic magmas in intra-oceanic island-arc settings. Although melting–assimilation–storage–homogenization (MASH) processes are common within volcanic arcs (DeBari and Greene, 2011; Jagoutz and Kelemen, 2015), it appears that juvenile magmas represented by LP IOAG can be generated by multi-step fractionation of depleted mantle melts at nearly closed-system conditions.

## 6. Conclusions

(1) The Davle volcanic complex trondhjemites, representing a subvolcanic member of a Neoproterozoic volcanic arc formed within the Cadomian–Avalonian accretionary orogen, resemble the most felsic members of the tonalite–trondhjemite suites from better exposed Phanerozoic intra-oceanic arcs in their composition.

(2) As revealed by inverse geochemical modelling, partial melting (either dehydration or water-excess) of mafic lower crust is an unlikely process to directly generate juvenile felsic melts

represented by the DVC trondhjemite. By contrast, the DVC trondhjemite was rather formed through fractional crystallization of intermediate magma of tonalitic composition which originated either from fractional crystallization or dehydration partial melting of a mafic precursor.

(3) Voluminous tonalite–trondhjemite plutonic suites commonly present within island arcs can form by low-pressure fractionation from mafic sources with no significant input of melts from the subducting plate or assimilation of an older arc crust. This process may be a dominant process governing the post-Archean crustal growth, and – together with the MASH processes – may account for the heterogeneity of magmatic rocks observed within volcanic arcs.

## Declaration of Competing Interest

The authors declare that they have no known competing financial interests or personal relationships that could have appeared to influence the work reported in this paper.

## Acknowledgments

We are grateful to Ladislav Strnad (Faculty of Science, Charles University; FS CU) for bulk-rock major and trace element analyses, Martin Racek (FS CU) for acquiring CL images, Jakub Trubač (FS CU) and Ladislav Polák (Institute of Geology of the Czech Academy of Sciences; IG CAS) for assistance with Hf isotopic analyses and Jan Rejšek (IG CAS) for Nd isotopic measurements. Karel Breiter (IG CAS) is acknowledged for helpful discussions on possible metasomatic effects. This paper was supported by the Czech Science Foundation project 20-13644S to LA, the Scientific Programme RVO67985831 of the Institute of Geology of the Czech Academy of Sciences and by the Center for Geosphere Dynamics (UNCE/SCI/006). We thank Vojtěch Janoušek and an anonymous reviewer for their constructive comments and Greg Shellnut for editorial handling. Their thorough work helped to improve the original manuscript significantly.

## Appendix A. Supplementary data

Supplementary data to this article can be found online at https://doi.org/10.1016/j.lithos.2022.106808.

## References

Ackerman, L., Bizimis, M., Haluzová, E., Sláma, J., Svojtka, M., Hirajima, T., Erban, V., 2016. Re-Os and Lu-Hf isotopic constraints on the formation and age of mantle pyroxenites from the Bohemian Massif. Lithos 256–257, 197–210.
Ackerman, L., Hajná, J., Žák, J., Erban, V., Sláma, J., Polák, L., Kachlík, V., Strnad, L., Trubač, J., 2019. Architecture and composition of ocean floor subducted beneath northern Gondwana during Neoproterozoic to Cambrian : a palinspastic reconstruction based on Ocean Plate Stratigraphy (OPS). Gondwana Res. 76, 77–97.
Ackerman, L., Pašava, J., Žák, J., Žák, K., Kachlík, V., Šebek, O., Trubač, J., Svojtka, M., Veselovský, F., Strnad, L., Santolík, V., 2021. Arc-related black shales as sedimentary archives of Sea-level fluctuations and plate tectonics during the late neoproterozoic: an example from the Bohemian Massif. Mar. Pet. Geol. 123, 104713.
Beard, J.S., 1995. Experimental, geological, and geochemical constraints on the origins of low-K silicic magmas in oceanic arcs. J. Geophys. Res. 100, 15593–15600.
Beard, J.S., Lofgren, G.E., 1991. Dehydration melting and water-saturated melting of basaltic and andesitic greenstones and amphibolites at 1, 3, and 6.9 kb. J. Petrol. 32, 365–401.
Bédard, J.H., 2006. A catalytic delamination-driven model for coupled genesis of Archaean crust and sub-continental lithospheric mantle. Geochim. Cosmochim. Acta 70, 1188–1214.
Blatter, D.L., Sisson, T.W., Hankins, W.B., 2013. Crystallization of oxidized, moderately hydrous arc basalt at mid- to lower-crustal pressures: Implications for andesite genesis. Contrib. Mineral. Petrol. 166, 861–886.
Brophy, J.G., 2008. A study of rare earth element (REE)-$SiO_2$ variations in felsic liquids generated by basalt fractionation and amphibolite melting: a potential test for discriminating between the two different processes. Contrib. Mineral. Petrol. 156, 337–357.
Calvert, A.J., 2011. The seismic structure of island arc crust. In: Brown, D., Ryan, P.D. (Eds.), Arc-Continent Collision. Springer, Berlin, Heidelberg, pp. 87–119.
Castillo, P.R., 2012. Adakite petrogenesis. Lithos 134–135, 304–316.
Chen, Y., Niu, Y., Al, C.E.T., 2019. Petrogenesis of ODP hole 735B (Leg 176) oceanic plagiogranite : Partial melting of gabbros or advanced extent of fractional crystallization? Geochem. Geophys. Geosyst. 20, 2717–2732.
Chin, E.J., Shimizu, K., Bybee, G.M., Erdman, M.E., 2018. On the development of the calc-alkaline and tholeiitic magma series: a deep crustal cumulate perspective. Earth and Planetary Science Letters 482, 277–287.
Cocherie, A., 1986. Systematic use of trace element distribution patterns in log-log diagrams for plutonic suites. Geochim. Cosmochim. Acta 50, 2517–2522.
Collett, S., Schulmann, K., Deiller, P., Štípská, P., Peřestý, V., Ulrich, M., Jiang, Y., Hoÿm de Marien, L., Míková, J., 2022. Reconstruction of the mid-Devonian HP-HT metamorphic event in the Bohemian Massif (European Variscan belt). Geosci. Front. 13, 1–19.
Davidson, J., Turner, S., Plank, T., 2013. Dy/Dy*: Variations arising from mantle sources and petrogenetic processes. J. Petrol. 54, 525–537.
DeBari, S.M., Greene, A.R., 2011. Vertical stratification of composition, density, and inferred magmatic processes in exposed arc crustal sections. In: Brown, D., Ryan, P. D. (Eds.), Arc-Continent Collision. Springer, Berlin, Heidelberg, pp. 121–144.
Dempírová, L., Šikl, J., Kašičková, R., Zoulková, V., Kříbek, B., 2010. The Evaluation of Precision and Relative Error of the Main Components of Silicate Analyses in Central Laboratory of the Czech Geological Survey. Geoscience Research Reports for 2009, pp. 326–330.
Dörr, W., Zulauf, G., Fiala, J., Franke, W., Vejnar, Z., 2002. Neoproterozoic to early Cambrian history of an active plate margin in the Teplá-Barrandian unit - a correlation of U-Pb isotopic-dilution-TIMS ages (Bohemia, Czech Republic). Tectonophysics 352, 65–85.
Drost, K., Gerdes, A., Jeffries, T., Linnemann, U., Storey, C., 2011. Provenance of Neoproterozoic and early Paleozoic siliciclastic rocks of the Teplá-Barrandian unit (Bohemian Massif): evidence from U-Pb detrital zircon ages. Gondwana Res. 19, 213–231.
D'Souza, R.J., Canil, D., Creaser, R.A., 2016. Assimilation, differentiation, and thickening during formation of arc crust in space and time: the Jurassic Bonanza arc, Vancouver Island, Canada. Bull. Geol. Soc. Am. 128, 543–557.
Faryad, S.W., Kachlík, V., 2013. New evidence of blueschist facies rocks and their geotectonic implication for Variscan suture(s) in the Bohemian Massif. J. Metamorph. Geol. 31, 63–82.
Fediuk, F., 2004. Alaskites and related rocks in the Proterozoic Jílové belt of Central Bohemia. Krystalinikum 30, 27–50.
Foley, S.F., Barth, M.G., Jenner, G.A., 2000. Rutile/melt partition coefficients for trace elements and an assessment of the influence of rutile on the trace element characteristics of subduction zone magmas. Geochim. Cosmochim. Acta 65, 933–938.
Franke, W., 2006. The Variscan orogen in Central Europe: Construction and collapse. Geol. Soc. Mem. 32, 333–343.
Freund, S., Haase, K.M., Keith, M., Beier, C., Garbe-Schönberg, D., 2014. Constraints on the formation of geochemically variable plagiogranite intrusions in the Troodos Ophiolite, Cyprus. Contrib. Mineral. Petrol. 167, 1–22.
Frost, B.R., Barnes, C.G., Collins, W.J., Arculus, R.J., Ellis, D.J., Frost, C.D., 2001. A geochemical classification for granitic rocks. J. Petrol. 42, 2033–2048.
Frost, C.D., Frost, B.R., Beard, J.S., 2016. On silica-rich granitoids and their eruptive equivalents. Am. Mineral. 101, 1268–1284.
Gill, J.B., 1981. Orogenic Andesites and Plate Tectonics. Springer-Verlag.
Greene, A.R., DeBari, S.M., Kelemen, P.B., Blusztajn, J., Clift, P.D., 2006. A detailed geochemical study of island Arc crust: the Talkeetna Arc section, south-Central Alaska. J. Petrol. 47, 1051–1093.
Hajná, J., Žák, J., Kachlík, V., 2011. Structure and stratigraphy of the Teplá-Barrandian Neoproterozoic, Bohemian Massif: a new plate-tectonic reinterpretation. Gondwana Res. 19, 495–508.
Hajná, J., Žák, J., Kachlík, V., 2014. Growth of accretionary wedges and pulsed ophiolitic mélange formation by successive subduction of trench-parallel volcanic elevations. Terra Nova 26, 322–329.
Hajná, J., Žák, J., Dörr, W., Kachlík, V., Sláma, J., 2018. New constraints from detrital zircon ages on prolonged, multiphase transition from the Cadomian accretionary orogen to a passive margin of Gondwana. Precambrian Res. 317, 159–178.
Jagoutz, O.E., 2010. Construction of the granitoid crust of an island arc. Part II: a quantitative petrogenetic model. Contrib. Mineral. Petrol. 160, 359–381.
Jagoutz, O., Kelemen, P.B., 2015. Role of arc processes in the formation of continental crust. Annu. Rev. Earth Planet. Sci. 43, 363–404.
Janoušek, V., Farrow, C.M., Erban, V., 2006. Interpretation of whole-rock geochemical data in igneous geochemistry: introducing Geochemical Data Toolkit (GCDkit). J. Petrol. 47, 1255–1259.
Jochum, K.P., Nohl, U., 2008. Reference materials in geochemistry and environmental research and the GeoReM database. Chem. Geol. 253, 50–53.
Kawate, S., Arima, M., 1998. Petrogenesis of the Tanzawa plutonic complex, Central Japan: Exposed felsic middle crust of the Izu–Bonin–Mariana arc. Island Arc 7, 342–358.
Kelemen, P.B., Hanghøj, K., Greene, A.R., 2003. One view of the geochemistry of subduction-related magmatic arcs, with an emphasis on primitive andesite and lower crust. Treat. Geochem. 3–9, 2–70.
Kříbek, B., Pouba, Z., Skoček, V., Waldhauserová, J., 2000. Neoproterozoic of the Teplá–Barrandian Unit as a part of the Cadomian orogenic belt: a review and correlation aspects. Bull. Czech Geol. Surv. 75, 175–196.
Le Bas, M.J., Le Maitre, R.N., Streckeisen, A., Zanettin, B., 1986. A chemical classification of volcanic rocks based on the total alkali-silica diagram. J. Petrol. 27, 745–750.

Leat, P.T., Larter, R.D., Millar, I.L., 2007. Silicic magmas of Protector Shoal, South Sandwich arc: Indicators of generation of primitive continental crust in an island arc. Geol. Mag. 144, 179–190.
Marien, C.S., Drewes-Todd, E.K., Stork, A., Todd, E., Gill, J.B., Hoffmann, J.E., Tani, K., Allen, C.M., Münker, C., 2022. Juvenile continental crust evolution in a modern oceanic arc setting: Petrogenesis of Cenozoic felsic plutons in Fiji, SW Pacific. Geochimica et Cosmochimica Acta 320, 339–365.
Martin, H., 1986. Effect of steeper Archean geothermal gradient on geochemistry of subduction-zone magmas. Geology 14, 753–756.
Martin, H., Smithies, R.H., Rapp, R., Moyen, J.F., Champion, D., 2005. An overview of adakite, tonalite-trondhjemite-granodiorite (TTG), and sanukitoid: Relationships and some implications for crustal evolution. Lithos 79, 1–24.
McDonough, W.F., Sun, S.S., 1995. The composition of the Earth. Chem. Geol. 120, 223–253.
Morávek, P., Röhlich, P., 1971. Geology of the northern part of the Jílové zone. Sborník Geologických věd 20, 101–141.
Moyen, J.F., 2009. High Sr/Y and La/Yb ratios: the meaning of the "adakitic signature". Lithos 112, 556–574.
Moyen, J.F., Martin, H., 2012. Forty years of TTG research. Lithos 148, 312–336.
Moyen, J.F., Janoušek, V., Laurent, O., Bachmann, O., Jacob, J.B., Farina, F., Fiannacca, P., Villaros, A., 2021. Crustal melting vs. fractionation of basaltic magmas: part 1, granites and paradigms. Lithos 402–403, 1–17.
Nakajima, K., Arima, M., 1998. Melting experiments on hydrous low-K tholeiite: Implications for the genesis of tonalitic crust in the Izu-Bonin-Mariana arc. Island Arc 7, 359–373.
Nandedkar, R.H., Ulmer, P., Müntener, O., 2014. Fractional crystallization of primitive, hydrous arc magmas: an experimental study at 0.7 GPa. Contrib. Mineral. Petrol. 167, 1–27.
O'Connor, J., 1965. A Classification for Quartz-Rich Igneous Rocks Based on Feldspar Ratios. US Geological Survey Proffetional Paper B, 525, pp. 79–84.
Patchett, J., Tatsumoto, M., 1980. Hafnium Isotope Variations in Oceanic Basalts. Geophys. Res. Lett. 7, 1077–1080.
Pearce, J.A., 1982. Trace element characteristics of lavas from destructive plate boundaries. In: Thorpe, R.S. (Ed.), Orogenic Andesites and Related Rocks. John Willey & Sons, Chichester, pp. 525–548.
Pearce, J.A., 2008. Geochemical fingerprinting of oceanic basalts with applications to ophiolite classification and the search for Archean oceanic crust. Lithos 100, 14–48.
Pearce, J.A., Harris, N.B.W., Tindle, A.G., 1984. Trace element discrimination diagrams for the tectonic interpretation of granitic rocks. J. Petrol. 25, 956–983.
Phelps, D., Avé Lallemant, H.G., 1980. The Sparta ophiolite complex, Northeast Oregon: a plutonic equivalent to low $K_2O$ island-arc volcanism. Am. J. Sci. 280, 345–358.
Pin, C., Gannoun, A., Dupont, A., 2014. Rapid, simultaneous separation of Sr, Pb, and Nd by extraction chromatography prior to isotope ratios determination by TIMS and MC-ICP-MS. J. Anal. At. Spectrom. 29, 1858–1870.
Plümper, O., Putnis, A., 2009. The complex hydrothermal history of granitic rocks: Multiple feldspar replacement reactions under subsolidus conditions. J. Petrol. 50, 967–987.
Rapp, R.P., Watson, E.B., 1995. Dehydration melting of metabasalt at 8-32 kbar: Implications for continental growth and crust-mantle recycling. J. Petrol. 36, 891–931.
Röhlich, P., 1998. The jílové belt: a Neoproterozoic volcanic rift zone in Central Bohemia. Acta Univ. Carol. Geol. 42, 489–493.
Rollinson, H.R., 1993. Using Geochemical Data. Longman, London.
Rollinson, H.R., 2009. New models for the genesis of plagiogranites in the Oman ophiolite. Lithos 112, 603–614.
Rong, J., Wang, F., 2016. Metasomatic Textures in Granites. Springer, Singapore.
Salters, V.J.M., 1996. The generation of mid-ocean ridge basalts from the Hf and Nd isotope perspective. Earth Planet. Sci. Lett. 141, 109–123.
Salters, V.J.M., Hart, S.R., 1991. The mantle sources of ocean ridges, islands and arcs: the Hf-isotope connection. Earth Planet. Sci. Lett. 104, 364–380.
Sláma, J., Dunkley, D.J., Kachlík, V., Kusiak, M.A., 2008. Transition from island-arc to passive setting on the continental margin of Gondwana: U-Pb zircon dating of Neoproterozoic metaconglomerates from the SE margin of the Teplá-Barrandian Unit, Bohemian Massif. Tectonophysics 461, 44–59.
Stern, R.J., Scholl, D.W., 2010. Yin and yang of continental crust creation and destruction by plate tectonic processes. Int. Geol. Rev. 52, 1–31.
Strnad, L., Mihaljevic, M., Sebek, O., 2005. Laser ablation and solution ICP-MS determination of rare earth elements in USGS BIR-1G, BHVO-2G and BCR-2G glass reference materials. Geostand. Geoanal. Res. 29, 303–314.
Vervoort, J.D., Patchett, P.J., Blichert-Toft, J., Albarède, F., 1999. Relationships between Lu-Hf and Sm-Nd isotopic systems in the global sedimentary system. Earth Planet. Sci. Lett. 168, 79–99.
Waldhauserová, J., 1984. Proterozoic volcanics and intrusive rocks of the Jílové zone in Central Bohemia. Krystalinikum 17, 77–97.
Zachariáš, J., Žák, K., Pudilová, M., Snee, L.W., 2013. Multiple fluid sources/pathways and severe thermal gradients during formation of the Jílové orogenic gold deposit, Bohemian Massif, Czech Republic. Ore Geol. Rev. 54, 81–109.
Žák, J., Sláma, J., 2018. How far did the Cadomian 'terranes' travel from Gondwana during early Palaeozoic? A critical reappraisal based on detrital zircon geochronology. Int. Geol. Rev. 60, 319–338.
Žák, J., Verner, K., Janoušek, V., Holub, F.V., Kachlík, V., Finger, F., Hajná, J., Tomek, F., Vondrovic, L., Trubač, J., 2014. A plate-kinematic model for the assembly of the Bohemian Massif constrained by structural relationships around granitoid plutons. Geol. Soc. Spec. Publ. 405, 169–196.
Zheng, X., Liu, Y., Zhang, L., 2021. The role of sulfate-, alkali-, and halogen-rich fluids in mobilization and mineralization of rare earth elements: Insights from bulk fluid compositions in the Mianning–Dechang carbonatite-related REE belt, southwestern China. Lithos 386–387 (106008).